Dual T cell– and B cell–intrinsic deficiency in humans with biallelic *RLTPR* mutations

Yi Wang,[1,3] Cindy S. Ma,[4,5]* Yun Ling,[1,3]* Aziz Bousfiha,[6]* Yildiz Camcioglu,[7]* Serge Jacquot,[8,9]* Kathryn Payne,[4] Elena Crestani,[10] Romain Roncagalli,[12] Aziz Belkadi,[1,3] Gaspard Kerner,[1,3] Lazaro Lorenzo,[1,3] Caroline Deswarte,[1,3] Maya Chrabieh,[1,3] Etienne Patin,[13,14] Quentin B. Vincent,[1,3] Ingrid Müller-Fleckenstein,[15] Bernhard Fleckenstein,[15] Fatima Ailal,[6] Lluis Quintana-Murci,[13,14] Sylvie Fraitag,[16] Marie-Alexandra Alyanakian,[17] Marianne Leruez-Ville,[18] Capucine Picard,[1,3,20] Anne Puel,[1,3] Jacinta Bustamante,[1,3,20] Stéphanie Boisson-Dupuis,[1,3,21] Marie Malissen,[12]** Bernard Malissen,[12]** Laurent Abel,[1,3]** Alain Hovnanian,[2,3]** Luigi D. Notarangelo,[10,11]** Emmanuelle Jouanguy,[1,3,21]*** Stuart G. Tangye,[4,5]*** Vivien Béziat,[1,3]*** and Jean-Laurent Casanova[1,3,19,21,22]***

[1]Laboratory of Human Genetics of Infectious Diseases, Necker Branch and [2]Laboratory of Genetic Skin Diseases: from Disease Mechanism to Therapies, Institut National de la Santé et de la Recherche Médicale U1163, 75015 Paris, France
[3]Paris Descartes University, Imagine Institute, 75015 Paris, France
[4]Immunology Division, Garvan Institute of Medical Research, Darlinghurst, Sydney, NSW 2010, Australia
[5]St. Vincent's Clinical School, University of New South Wales, Darlinghurst, Sydney, NSW 2010, Australia
[6]Clinical Immunology Unit, Casablanca Children's Hospital, Ibn Rochd Medical School, King Hassan II University, Casablanca 20100, Morocco
[7]Division of Infectious Diseases, Clinical Immunology, and Allergy, Department of Pediatrics, Cerrahpaşa Medical Faculty, Istanbul University, 34452 Istanbul, Turkey
[8]Immunology Unit, Rouen University Hospital, 76031 Rouen, France
[9]Institut National de la Santé et de la Recherche Médicale U905, Institute for Research and Innovation in Biomedicine, Rouen Normandy University, 76183 Rouen, France
[10]Division of Immunology, Boston Children's Hospital, Boston, MA 02115
[11]Harvard Stem Cell Institute, Harvard University, Cambridge, MA 02138
[12]Center for Immunology Marseille-Luminy, 13288 Marseille, France
[13]Human Evolutionary Genetics Unit, Institut Pasteur, 75015 Paris, France
[14]Centre National de la Recherche Scientifique URA 3012, 75015 Paris, France
[15]Institute of Clinical and Molecular Virology, University of Erlangen-Nürnberg, D-91054 Erlangen, Germany
[16]Department of Pathology, [17]Immunology Unit, [18]Virology Laboratory, Paris Descartes University, Sorbonne Paris Cité-EA 36–20, [19]Pediatric Hematology-Immunology Unit, and [20]Center for the Study of Primary Immunodeficiencies, Necker Hospital for Sick Children, Assistance Publique - Hôpitaux de Paris, 75015 Paris, France
[21]St. Giles Laboratory of Human Genetics of Infectious Diseases, Rockefeller Branch and [22]Howard Hughes Medical Institute, The Rockefeller University, New York, NY 10065

Combined immunodeficiency (CID) refers to inborn errors of human T cells that also affect B cells because of the T cell deficit or an additional B cell–intrinsic deficit. In this study, we report six patients from three unrelated families with biallelic loss-of-function mutations in *RLTPR*, the mouse orthologue of which is essential for CD28 signaling. The patients have cutaneous and pulmonary allergy, as well as a variety of bacterial and fungal infectious diseases, including invasive tuberculosis and mucocutaneous candidiasis. Proportions of circulating regulatory T cells and memory CD4$^+$ T cells are reduced. Their CD4$^+$ T cells do not respond to CD28 stimulation. Their CD4$^+$ T cells exhibit a "Th2" cell bias ex vivo and when cultured in vitro, contrasting with the paucity of "Th1," "Th17," and T follicular helper cells. The patients also display few memory B cells and poor antibody responses. This B cell phenotype does not result solely from the T cell deficiency, as the patients' B cells fail to activate NF-κB upon B cell receptor (BCR) stimulation. Human RLTPR deficiency is a CID affecting at least the CD28-responsive pathway in T cells and the BCR-responsive pathway in B cells.

INTRODUCTION

Inborn errors of human T cell development or function comprise an expanding group of primary immunodeficiencies (PIDs; Zhang et al., 2015). Severe combined immunodeficiency (CID [SCID]) is defined by an absence of autologous T cells. SCID is characterized by a wide variety of life-threatening infections in early childhood (Buckley, 2004; Picard et al., 2015). In contrast, the term CID is used to define related conditions in which T cells are present but their development

*C.S. Ma, Y. Ling, A. Bousfiha, Y. Camcioglu, and S. Jacquot contributed equally to this paper.

**M. Malissen, B. Malissen, L. Abel, A. Hovnanian, and L.D. Notarangelo contributed equally to this paper.

***E. Jouanguy, S.G. Tangye, V. Béziat, and J.-L. Casanova contributed equally to this paper.

Correspondence to Vivien Béziat: vivien.beziat@inserm.fr

Abbreviations used: 3D, three dimensional; Ab, antibody; AR, autosomal recessive; BCG, bacille Calmette-Guérin; BCR, B cell receptor; CID, combined immunodeficiency; HD, homodimerization domain; ICOS, inducible T cell co-stimulator; IVIG, intravenous IgG; LOD, logarithm of the odds; LRR, leucine-rich repeat; MAF, minor allele frequency; MAIT cell, mucosal-associated invariant T cell; MFI, mean fluorescence intensity; NGFR, nerve growth factor receptor; PID, primary immunodeficiency; qRT-PCR, quantitative real-time PCR; RAR, relative auto-Ab reactivity; SCID, severe CID; SNP, single nucleotide polymorphism; Tfh cell, T follicular helper cell; WES, whole-exome sequencing.

The Rockefeller University Press $30.00
J. Exp. Med. 2016 Vol. 213 No. 11 2413–2435
www.jem.org/cgi/doi/10.1084/jem.20160576

and/or function is impaired, and antibody (Ab) responses are also affected (Notarangelo, 2014). The B cell phenotype can be a consequence of the T cell deficit or of an additional B cell–intrinsic defect. Patients with CID suffer from various infections and often also from autoimmunity, allergy, or both. Autoinflammatory and proliferative phenotypes are more rarely observed. A growing number of T cell disorders do not fall into these two categories because of an apparently intact B cell compartment and normal Ab responses. Distinctive laboratory and clinical features distinguish patients with various T cell immunodeficiencies. Each PID, and as a matter of fact each patient with a PID, is an experiment of nature, the elucidation of which connects an inborn error of immunity with a set of phenotypes as they develop in natural conditions (medical care evidently altering the course of maladies), as opposed to experimental conditions (iatrogenic diseases not being properly experimental; Casanova and Abel, 2004; Casanova et al., 2014).

The analysis of T cell immunity to infection has benefited from such genetic studies. For example, inborn errors of T cell immunity mediated by IFN-γ, the T helper cell 1 (Th1 cell) signature cytokine in inbred mice, were shown to underlie Mendelian susceptibility to mycobacterial disease (O'Shea and Paul, 2010; Bustamante et al., 2014). Conversely, inborn errors of IL-17A/F, the Th17 signature cytokines, underlie chronic mucocutaneous candidiasis (Puel et al., 2012). For both conditions, cells other than $CD4^+$ Th lymphocytes are affected. T cells can be implicated in the pathogenesis of infections caused by *Mycobacterium* and *Candida* because they occur in patients with pure forms of SCID, in which only T cells are intrinsically affected. Their occurrence in children with a selective defect of $CD4^+$ Th lymphocytes caused by MHC class II deficiency is less well documented. Inborn errors of $CD8^+$ T cells can disrupt immunity to specific viruses, as exemplified by X-linked lymphoproliferative disease caused by inactivating mutations in *SH2D1A* encoding SAP (Tangye, 2014). Cytotoxic T cells in males with SAP deficiency cannot control EBV-infected B cells (Tangye, 2014). However, some infections cannot yet be ascribed to specific disorders of T cells. For example, the mechanisms by which human T cells control staphylococci are unclear. Staphylococcal infections, commonly seen in patients with disorders of phagocytes, are also often associated with inborn errors of IL-17A/F (Ma et al., 2008; Milner et al., 2008; Puel et al., 2011), severe allergy (Aydin et al., 2015), or impaired IL-6 immunity (Puel et al., 2008; Kreins et al., 2015). We studied six patients from three unrelated kindreds with unusual histories of mycobacterial diseases, mucocutaneous candidiasis, silent but detectable EBV viremia, and/or staphylococcal diseases in the context of pulmonary and cutaneous allergy. We tested the hypothesis that they suffered from a novel T cell deficit.

RESULTS

Clinical phenotypes of the patients

We investigated six patients from three kindreds (Fig. 1 a, Fig. S1, Table 1, and Case studies section of Materials and methods). A1, A2, and A3 (kindred A) were born to consanguineous parents in Morocco. A1 suffered from various infections, including mucocutaneous candidiasis (onyxis and perionyxis of almost all fingers and toes) from age 5 yr onward, and from multifocal tuberculosis (affecting cervical lymph nodes as well as the respiratory and digestive tracts) at 8 yr. He died at age 17 from respiratory distress. A2 and A3 are 2-yr-old dizygotic twin sisters who suffer from mucocutaneous candidiasis (onyxis and perionyxis of almost all fingers and toes; Fig. 1 b) and recurrent bacterial infections of the lung. B1 and B2 (kindred B) are now aged 27 and 26 yr and were born to consanguineous parents originating from Tunisia. They have lived in France and suffered from asthma, subcutaneous staphylococcal abscesses (Fig. 1 b), and recurrent infections of the upper and lower respiratory tracts. C1 (kindred C) was born to nonconsanguineous parents in Turkey, where he lived and suffered from miliary tuberculosis at age 9 yr. He is now aged 18 and is doing well. At last follow up, B1 was treated with intravenous IgG (IVIG), whereas A2, A3, B2, and C1 were not receiving any treatment. All patients were born with normal skin but gradually developed clinical manifestations, including severe allergic lesions (Table 1, Fig. S1, and Case studies section of Materials and methods). Histological analysis of a skin biopsy from B2 showed psoriasiform hyperplastic epidermis and spongiosis, with superficial perivascular infiltrate mostly containing $CD8^+$ T cells (Fig. 1 c and not depicted). No severe illnesses caused by common viruses, including herpes viruses, were reported in these patients as inferred from viral serologies (Table S1). Interestingly, EBV viremia was documented in four of the six patients (Table S2), although they did not display any EBV-related clinical manifestations. Overall, these patients suffered from a broad and partly overlapping phenotype of recurrent infectious diseases caused by multiple pathogens, including *Mycobacterium*, *Staphylococcus*, and *Candida* in the context of cutaneous and pulmonary allergy.

Identification of rare biallelic *RLTPR* mutations

We analyzed the patients collectively by genome-wide linkage and whole-exome sequencing (WES). Multipoint linkage analysis was performed for the two consanguineous kindreds (A and B) with a model of affected siblings only. The maximum logarithm of the odds (LOD) scores (2.53 for kindred A and 2.0556 for kindred B) were obtained for an overlapping region of 3.2 Mb on chromosome 16 (Fig. S2 a). Only one of the 141 protein-coding genes in the linked region, *RLTPR*, also known as *CARMIL2*, carried homozygous rare variants in all five patients of kindred A and B, as detected by WES. In addition, the high homozygosity rate (3–4%) in C1 was strongly suggestive of parental consanguinity (Fig. S2 b; Belkadi et al., 2016). The region encompassing *RLTPR* was homozygous in C1, who carried a homozygous rare variant in *RLTPR*. Noteworthy, the mouse orthologue of this gene is essential for CD28 costimulation of T cells (Liang et al., 2013). We confirmed these variants by Sanger sequencing (Fig. 1 d). A1, A2, and A3 carry a homozygous nucleotide substitution

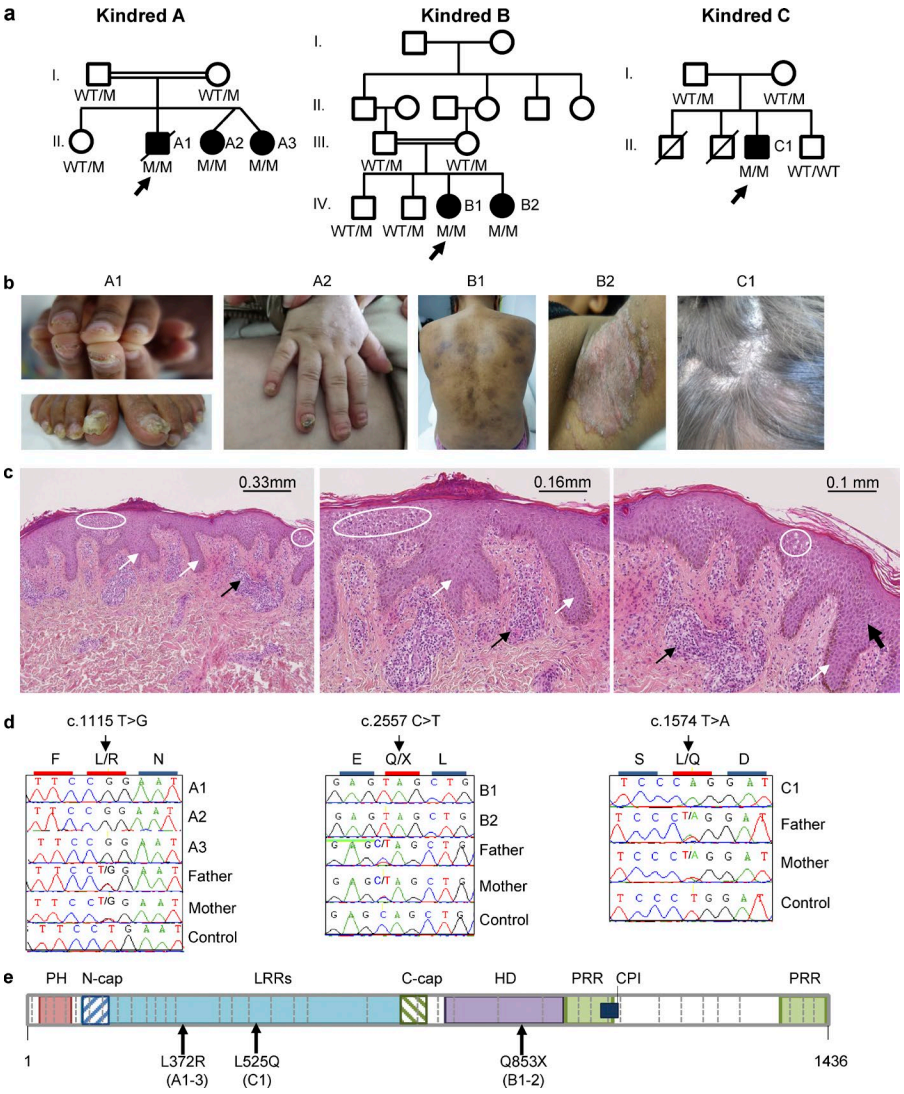

Figure 1. **AR RLTPR deficiency.** (a) Pedigrees of three families showing the familial segregation of the L372R, Q853X, and L525Q mutant *RLTPR* alleles. Kindreds are designated by A, B, and C. Generations are designated by Roman numerals (I, II, and III). A1, A2, A3, B1, B2, and C1 are represented by black symbols; the proband is indicated by an arrow. (b) Representative pictures of patients' skin phenotype: Onyxis and perionyxis of all fingers of A1 and A2, pigmented plaques on the back of B1, large inflammatory and ulcerative plaques in the left armpit of B2, and seborrheic dermatitis on the scalp of C1. (c) B2's inflammatory skin histology. (Left) Hyperplastic epidermis showing spongiosis accompanied by a slight lymphocytic exocytosis. There is a focal parakeratosis with crusting. (Middle) Psoriasiform hyperplastic epidermis with an overlying crust containing serosity and some neutrophils. A superficial perivascular infiltrate made up of lymphocytic cells is shown. (Right) Slightly spongiotic acanthotic epidermis with focal parakeratosis and lymphocytic perivascular infiltrate. White circles indicate spongiosis, thin black arrows indicate lymphocytic infiltrates, the thick black arrow indicates acanthosis, and white arrows indicate rete ridges. (d) Sequencing profiles showing the homozygous *RLTPR* c. 1115 T>G, p. L372R mutation of A1, A2, and A3; c. 2557 C>T, p. Q853X mutation of B1 and B2; c. 1574 T>A, p. L525Q of C1 in genomic DNA of patients, siblings, parents, and WT controls. (e) Schematic representation of the RLT PR protein. The different domains are depicted as follows: the pleckstrin homology (PH) domain in pink, the leucine-rich region (LRRs) in light blue, the HD in purple, the proline rich regions (PRR) in light green, and the CP-interacting (CPI) domain in black. The 38 exons are delineated by vertical dashed bars. The identified mutations and their amino acid positions are indicated by arrows. C-cap, C-terminal cap of the LRR; N-cap, N-terminal cap of the LRR.

(T>G) at position 1,115 in exon 14 of *RLTPR*, resulting in the replacement of a highly conserved leucine residue by an arginine (L372R) in the leucine-rich repeat (LRR) domain (Fig. 1, d and e; and Fig. S2 c). B1 and B2 carry a nucleotide substitution (C>T) at position 2,557 in exon 25, resulting in the replacement of a glutamine residue by a stop codon (Q853X; Fig. 1, d and e). C1 carries a homozygous nucleotide substitution (T>A) at position 1,574 in exon 17, resulting in the replacement of a highly conserved leucine residue with glutamine (L525Q; Fig. 1, d and e; and Fig. S2 c). The intrafamilial segregation of the *RLTPR* genotype and clinical phenotype in the three kindreds was consistent with an autosomal recessive (AR) trait with complete penetrance, as all parents and unaffected siblings were heterozygous or homozygous WT (Fig. 1 a). A1, A2, A3, and C1 carry mutations affecting conserved leucines of the LRR domain. This is similar to the L432P mutation in mouse RLTPR, which was previously shown to be loss of function (Liang et al., 2013). The combined annotation–dependent depletion scores of L372R (15.96), Q853X (38.6), and L525Q (29.22) are well above the mutation significance cutoff of RLTPR (10.05; Fig. S2 d; Kircher et al., 2014; Itan et al., 2016). None of the three variants was previously reported in 1000 Genomes, Single Nucleotide Polymorphism (SNP), HapMap, EVS, and ExAC databases, nor in the Greater Middle-Eastern variome (Scott et al., 2016) or in our own WES database of over 3,000 exomes. The minor allele frequency (MAF) of these three hitherto private alleles is therefore $<10^{-6}$. No other homozygous

Table 1. **Clinical phenotype of patients**

Patient, origin, gender, present age (yr)	Infectious diseases	Cutaneous features	Others	Level of IgE
				KIU/ml
A1				
Morocco	Purulent otitis	Scaly erythroderma	Bronchitis	<5
Male	Multifocal tuberculosis	Focal alopecia	Peptic stenosis of the esophagus	
Died at 17	Onychomycosis with perionyxis	Pustular-like and scaly lesions on the soles		
	CMC (perionyxis)			
A2				
Morocco	CMC (perionyxis and oral thrush)	Scaly erythroderma	Bilateral bronchoalveolar syndrome	<2
Female	Recurrent bacterial lung infections			
2				
A3				
Morocco	CMC (perionyxis)	Scaly erythroderma	Recurrent bacterial lung infections	<2
Female	Bilateral bronchoalveolar syndrome			
2				
B1				
Tunisia	Recurrent purulent otitis	Eczema	Bronchial dilatation	1,381
Female	Subcutaneous abscesses	Cold urticaria	Asthma	
27	Molluscum contagiosum	Lupus-like facial erythema	Allergy to yolk egg and peanut	
	Recurrent bacterial lung infections	Hyperpigmented lesions		
	Gastritis by Helicobacter pylori			
B2				
Tunisia	Pneumonia	Eczema	Recurrent bronchopneumonia	2.3
Female		Psoriasis guttata-like lesions	Bronchial dilatation	
26	Subcutaneous abscesses	Mild ichthyosis	Asthma	
		Sun intolerance		
	Molluscum contagiosum	Dry skin		
		Large inflammatory and erosive inverted psoriasis-like plaques in the folds		
C1				
Turkey	Miliary tuberculosis	Seborrheic dermatitis	Asthma	34.7
Male				
19				

CMC, chronic mucocutaneous candidiasis.

RLTPR nonsense, essential splicing, or frameshift deletion/insertion variations were found in these databases. Finally, the *RLTPR* gene has a medium gene damage index score of 4.938, a moderate neutrality index score, and purifying *f* parameter of 0.32 and 0.488, suggesting that *RLTPR* is under purifying selection (Fig. S2 e; Itan et al., 2015). Overall, both family and population genetic studies strongly suggested that these six patients had AR RLTPR deficiency.

Overexpression and dimerization of mutant human *RLTPR* alleles

We first tested the expression of RLTPR protein upon transient transfection of HEK293T cells with C-terminal Flag-tagged expression vectors carrying the WT or mutant *RLTPR* alleles (L372R, Q853X, and L525Q). In this overexpression system, we observed normal levels of both missense proteins, as assessed by Western blotting with two Abs (Fig. 2 a, left; commercial polyclonal anti–N-terminal anti-RLTPR and our C-terminal EM-53 mAb recognizing an epitope between residues 1,147 and 1,272 in the C-terminal region of RLTPR; see Roncagalli et al. in this issue). In contrast, the Q853X mutation resulted in expression of a truncated protein that was detected only with the anti–N-terminal RLTPR Ab (Fig. 2 a, right). RLTPR is a large multidomain protein of the CARMIL family, containing an LRR (residues 247–667) and a homodimerization domain (HD; residues 728–905, as predicted by homology with CARMIL1; Fig. 1 c; Matsuzaka et al., 2004). Interestingly, CARMIL1 dimerization occurs through both antiparallel HDs and contact between the two extremities of horseshoe-shaped LRRs (Zwolak et al., 2013). The canonical sequence of LRR motifs is LxxLxLxxN/CxL. L372 and L525 are both located at the second canonical position of their respective LRR motifs (Lxx**L**xLxxN/CxL; bold, underlined) and are both highly conserved across species (Fig. S2 c). The crystal structure of the LRR domain of CARMIL1 has been recently published (Zwolak et al., 2013). CARMIL1 has a 33.2% protein sequence identity (62% similarity) with RLTPR, with a 43.8% sequence identity (73.7% similarity) between their LRR domains but only 24% sequence identity (64.7% similarity) between their HD domains, as defined by LALIGN software (Huang and Miller, 1991; Liang et al., 2009; Zwolak et al., 2013). By inference from this structure, Q853 is located in the HD domain, and both L372 and L525 are predicted to localize at the center of the hydrophobic core of the

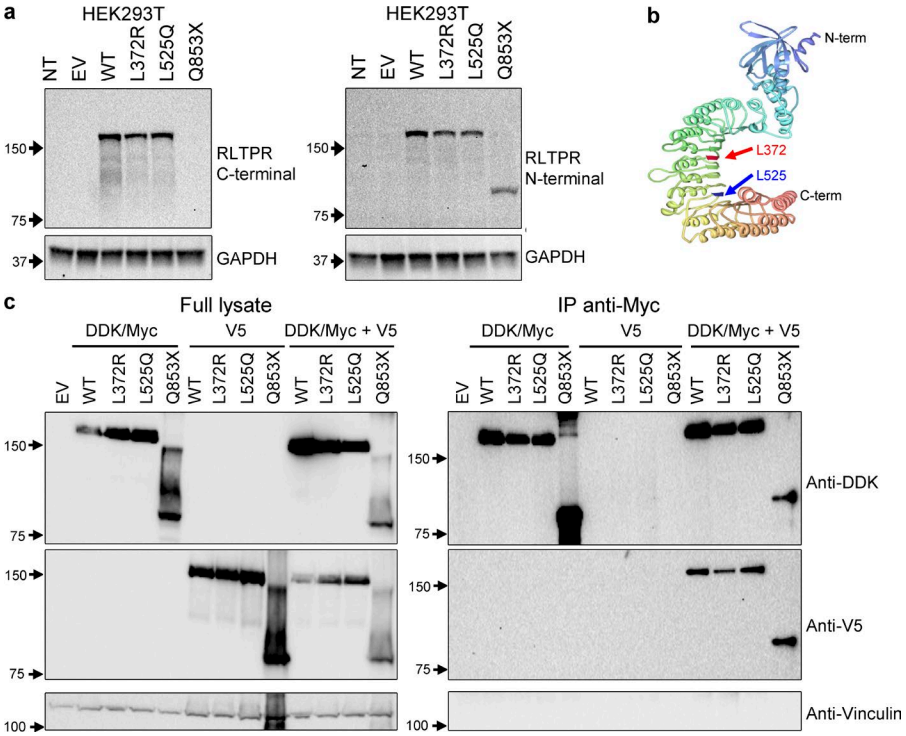

Figure 2. **Molecular characterization of RLTPR mutations.** (a) HEK293T cells were either mock-transfected (NT) or transfected with an empty pCMV6 plasmid (EV) or pCMV6 plasmids encoding RLTPR WT or L372R, L525Q, or Q853X RLTPR mutant alleles. Whole cell lysates were subjected to immunoblots against the indicated RLTPR domains. (b) 3D representation of the CARMIL family LRR region (Zwolak et al., 2013). The L372 and L525 residues are depicted in red and blue, respectively. C-term, C terminus; N-term, N terminus. (c) Effect of mutations on RLTPR homodimerization. HEK293T cells were transfected with RLTPR WT or L372R, L525Q, or Q853X RLTPR mutant alleles tagged in the C terminus with either V5 or Myc/DDK. Full cell lysates (left) or anti-Myc immunoprecipitates (IP; right) are depicted. Data are representative of three independent experiments. Molecular mass is shown in kD.

LRR domain. The lack of a C-terminal segment of the HD domain (Q853X) might prevent the dimerization, whereas substitutions of leucine to arginine or glutamine (L372R and L525Q) might thus destabilize the planar horseshoe shape of the LRR structure (Fig. 2 b). We assessed the capacity of the WT and mutated proteins to dimerize in HEK293T cells by cotransfecting these cells with DDK/Myc or V5 C-terminal–tagged version of WT or mutant RLTPR. Coimmunoprecipitation with the Myc-Ab showed that WT, L372R, L525Q, and Q853X proteins were capable of dimerization (Fig. 2 c). Overall, we show that human RLTPR can dimerize and that L372R, L525Q, and Q853X mutations do not impair dimerization, at least in this overexpression system. These data also suggest that the residues 853–905 of the predicted HD domain are not essential for dimerization. We cannot exclude that RLTPR can form oligomers and requires other protein partners to dimerize or oligomerize.

Decreased expression of RLTPR mutant proteins in the patients' cells

Next, we evaluated *RLTPR* expression at the mRNA and protein levels in control and patients' cells. By quantitative real-time PCR (qRT-PCR), no significant difference was observed in the amounts of *RLTPR* in EBV-transformed B cells (EBV-B cells) of A1, B2, and C1, as compared with healthy controls (Fig. 3 a). In contrast, higher or normal mRNA levels were observed in herpesvirus saimiri–transformed T cell lines (T-saimiri cells) of A1 and B1, respectively, as compared with healthy controls, suggesting that the nonsense mutation is not associated with significant nonsense-mediated mRNA decay (Fig. 3 b). We then assessed the amount of human RLTPR protein in EBV-B cells, T-saimiri cells, and PHA blasts from controls and patients by Western blotting using the in-house mAb EM-53 (Fig. 3, c–e; Roncagalli et al., 2016). The L372R (A1) and L525Q (C1) variants of RLTPR were expressed at much lower levels than WT proteins in EBV-B cells (20% and 35% of WT, respectively), T-saimiri cells (20% of WT for L372R), and PHA blasts (20% of WT for both). The truncated Q853X protein (B2) was not detectable in patient-derived EBV-B cells, T-saimiri cells, and PHA blasts as expected, with an Ab recognizing the C-terminal domain of RLTPR (Fig. 3, c–e). Unfortunately, none of the commercially available Abs recognizing the N-terminal domain of RLTPR detected endogenous RLTPR in control cells (not depicted). Thus, we cannot exclude the possibility that a truncated Q853X protein is expressed in the patients' cells. Stable transduction of WT *RLTPR* in T-saimiri cells of B1 restored normal expression of RLTPR, suggesting that the lack or poor expression of RLTPR was caused by *RLTPR* mutations (Fig. 3 f). Collectively, these data indicate that both missense RLTPR alleles are poorly expressed at the protein level in patients' cells, whereas the nonsense allele encodes a truncated protein, the levels of expression of which in the patients' cells are unknown.

WT and mutant RLTPR expression in circulating leukocytes

To test expression of mutant RLTPR in leukocytes ex vivo, we first analyzed the expression profile of WT RLTPR in $CD4^+$ and $CD8^+$ T cell subsets, B cells, NK cells, and $CD14^+$ monocytes from healthy controls by Western blotting with

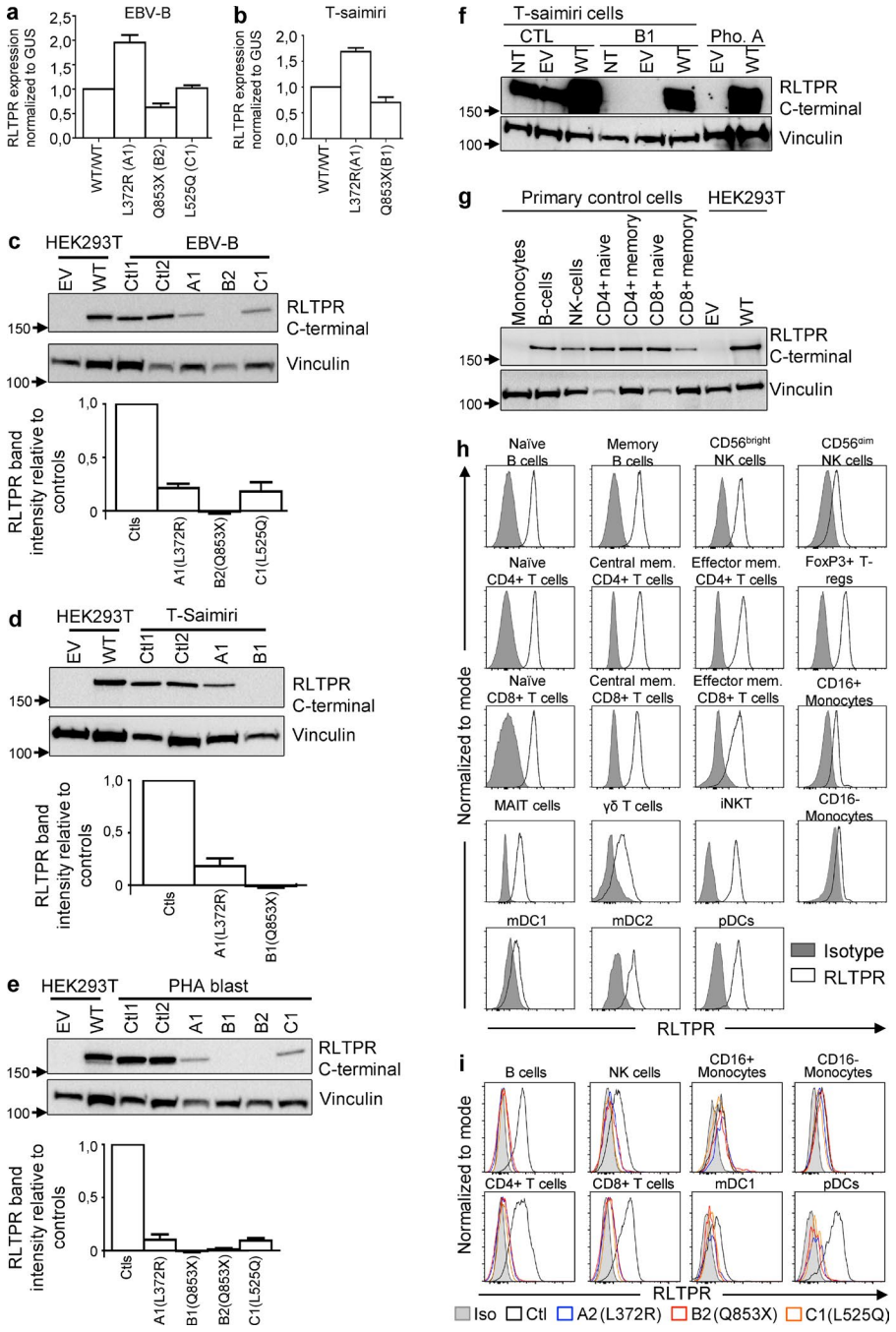

Figure 3. **RLTPR expression in patients' derived cells and leukocyte subsets.** (a) Relative quantification of *RLTPR* mRNA in EBV-B cells from three independent controls (WT/WT), A1, B2, and C1 (three independent replicates). (b) Relative quantification of *RLTPR* mRNA in T-Saimiri cells from three independent controls (WT/WT), A1, and B1 (three independent replicates). (a and b) Human *GUS* was used as an endogenous gene for comparison. The ratio of *RLTPR* to *GUS* mRNA levels is shown, and error bars indicate the standard deviation for each mutant independently. (c–e) Immunoblot analysis of RLTPR expression in whole protein extracts of HEK293T cells transfected with an empty pCMV6 plasmid (EV) or pCMV6 plasmids encoding WT RLTPR or in indicated patients' derived EBV-B cells (c; three independent replicates), T-Saimiri cells (d; four independent replicates), or PHA blasts (e; two to four independent replicates) and relative quantifications of RLTPR bands from controls (Ctl). Data are mean ± SD. (f) Immunoblot analysis of RLTPR expression in whole protein extracts of T-Saimiri cells from control or B1 not transduced (NT) or transduced with retrovirus encoding either a tag only (empty vector [EV]) or tagged WT RLTPR. Phoenix A (Pho. A) cells transfected with an empty pLZRS plasmid (EV) or pLZRS plasmid encoding WT RLTPR were used as controls. (g) Immunoblot analysis of RLTPR expression in whole protein extracts from monocytes, B cells, NK cells, $CD4^+$ T cells, and $CD8^+$ T cells of healthy controls and HEK293T overexpression controls. (f and g) Data are representative of three experiments. Molecular mass is shown in kD. (h) RLTPR expression determined by FACS in indicated leukocyte subsets from healthy controls. mDC, myeloid DC; mem. memory; pDCs, plasmacytoid DCs. (i) RLTPR expression determined by FACS in indicated leukocyte subsets from healthy control, A2, B2, and C1. Iso, isotypic control.

the EM-53 C-terminal mAb (Roncagalli et al., 2016). We detected strong expression of WT RLTPR in naive and memory $CD4^+$ and $CD8^+$ T cells, B cells, and NK cells, whereas it was poorly expressed in monocytes (Fig. 3 g). By flow cytometry, using the same EM-53 mAb, RLTPR expression was detected in naive and memory B cells, $CD56^{bright}$ and $CD56^{dim}$ NK cells, naive, central, and effector memory $CD4^+$ and $CD8^+$ αβ T cells, regulatory T cells (T reg cells), mucosal-associated invariant T cells (MAIT cells), γδ T cells, invariant NKT cells (iNKT cells), mDC2, and plasmacytoid DCs but only weakly detectable, if at all, in monocytes and mDC1 (Fig. 3 h). In the same experimental conditions, patients homozygous for the Q853X, L525Q, or L372R "mutations" did not display detectable RLTPR in any leukocyte population tested (Fig. 3 i). Consistent with assessment of RLTPR expression in total monocytes by Western blotting (Fig. 3 g), $CD14^{lo}CD16^+$ and $CD14^{hi}CD16^-$ monocytes from healthy controls lacked expression of RLTPR (Fig. 3 h) when compared with B2 cells carrying the premature stop codon Q853X in *RLTPR* and serving as a negative control

(Fig. 3 i). Collectively, these data indicate that the endogenous expression of the mutant RLTPR protein is even much lower in primary cells ex vivo than in PHA blasts and cell lines cultured in vitro. Expression studies in mice were consistent, and functional studies predicted at least an impact on T cells because of the role of RLTPR in CD28 signaling in mice (Liang et al., 2013; Roncagalli et al., 2016). Our studies also suggest that the patients may suffer from defects in T cells, B cells, NK cells, and possibly some myeloid subsets.

Development of leukocyte subsets in RLTPR-deficient individuals

We then assessed the effect that mutations in RLTPR had on the different compartments of circulating leukocytes by flow cytometry. All patients had normal counts of polymorphonuclear leukocytes (neutrophils and basophils), monocytes, B cells, and NK cells (Table S3). All patients except B1 had elevated counts of $CD8^+$ T cells. A1 and C1 had elevated counts of $CD4^+$ T cells. Increased counts of eosinophils were documented twice in B1 (Table S3). In addition, we observed increased frequencies of naive $CD4^+$ T cells and reduced frequencies of $CD45RA^-CCR7^+$ central memory $CD4^+$ and $CD8^+$ T cells (Fig. 4 a). Other subsets of memory T cells were not affected (Fig. 4 a). Flow cytometric analysis of T cell subsets ex vivo revealed normal proportions of γδ T cells, NKT cells, and Th2 ($CCR6^-CXCR3^-$) cells but significantly decreased proportions of T reg cells ($CD4^+FOXP3^+CD25^+CD127^{lo}$), T follicular helper cells (Tfh cells; $CD4^+CXCR5^+$), Th17 ($CD4^+CCR6^+CXCR3^-$) cells, and MAIT ($CD3^+CD161^+V\alpha7.2$) cells and a slight but nonsignificant decrease of Th1 cells ($CD4^+CXCR3^+CCR6^-$; Fig. 4, b–f). We further enumerated Th2-type cells by determining the proportions of memory $CD4^+$ T cells that expressed the surface receptor CRTh2, which is expressed on human $CD4^+$ T cells enriched for producing IL-4, IL-5, and IL-13 (Nagata et al., 1999; Cosmi et al., 2000). This analysis revealed normal proportions of $CRTh2^+$ cells within the memory $CD4^+$ T cell subsets in RLTPR-deficient patients compared with controls (3.2% in patients vs. 2.5% in controls; Fig. 4 g). Some of these T cell phenotypes were consistent with the patients' clinical manifestations, such as the occurrence of invasive tuberculosis and mucocutaneous candidiasis (low Th1 and Th17 cells, respectively; Puel et al., 2012; Bustamante et al., 2014) and cutaneous staphylococcal and pulmonary bacterial diseases (low Th17 and Tfh cells, respectively; Tangye et al., 2013; Ma et al., 2015), whereas others were apparently silent clinically (low T reg and MAIT cells).

Defective CD28 costimulation in the patients' $CD4^+$ T cells

Because RLTPR has been shown to have a nonredundant role in the CD28 costimulation pathway in mice (Liang et al., 2013), we tested the ability of patients' T cells to proliferate in vitro in response to various stimuli. T cell proliferation upon stimulation with PMA/ionomycin, PHA, or OKT3 (anti-CD3 mAb) activation was diminished in patients when compared with healthy controls (Table S4). Consistently, proliferation to recall antigens was also diminished (Table S4). This suggests that full T cell activation by OKT3 or recall antigens, in these experimental conditions, including the presence of antigen-presenting cells, requires an intact RLTPR, probably because of its requirement downstream of CD28 (which can be activated in this assay by antigen-presenting cells in the presence of OKT3 or PHA). Impaired responses to PMA/ionomycin probably reflects the low proportion of memory T cells in the patients, as control naive T cells do no proliferate as well as memory T cells in response to this stimulus (unpublished data). Mice homozygous for the L432P substitution in Rltpr ($Rltpr^{bas}$) resemble immunologically those lacking CD28 (Shahinian et al., 1993; Acuto and Michel, 2003). $Rltpr^{bas}$ mice have normal counts of $CD4^+$ and $CD8^+$ T cell subsets in peripheral blood, with the exception of strongly diminished T reg cells and $CD4^+$ memory T cells (Liang et al., 2013). Moreover, the synergistic impact of CD28 co-stimulation on TCR-mediated proliferation and IL-2 production is abolished in *$Rltpr^{bas}$* $CD4^+$ T cells. $CD8^+$ T cells are also affected, albeit to a lesser extent. In RLTPR-deficient patients, as defined by FACS mean fluorescence intensity (MFI), we found that the CD28 expression level was decreased on the surface of both naive and memory $CD4^+$ and $CD8^+$ T cells, compared with control naive and memory $CD4^+$ and $CD8^+$ T cells, respectively (Fig. S3, a and b). However, all naive and memory $CD4^+$ and all naive $CD8^+$ T cells express CD28, whereas the proportion of $CD28^+$ cells in memory $CD8^+$ T cells was significantly decreased in patients (Fig. S3 c). This likely reflects the diminished frequency of the central memory subset in patients' $CD8^+$ T cells, which all express CD28 (Romero et al., 2007). We then analyzed the CD28 co-stimulation pathway in all patients and healthy controls. Using a redirected triggering assay against the P815 cell line, we cross-linked CD3 and/or CD28 on T cells with specific mAbs for 6 h. This approach allowed us to assess the impact of CD3 and CD28 co-stimulation on IL-2, TNF, and IFN-γ intracellular production by $CD4^+$ T cells, as well as TNF and IFN-γ intracellular production and CD107a surface expression (a surrogate of vesicle degranulation) by $CD8^+$ T cells (Fig. 5, a and b; and Fig. S3, d and e). Because control naive $CD4^+$ and $CD8^+$ T cells respond poorly to CD3 and CD28 co-stimulation in these experimental conditions (Fig S3, d and e), we compared control and patients' memory cells (Fig. 5, a and b). CD3 stimulation alone induced little or no TNF, IFN-γ, and IL-2 in both control and patients' $CD4^+$ memory T cells (Fig. 5 a). CD3 and CD28 co-stimulation of control $CD4^+$ memory T cells strongly synergized for TNF and IL-2 and much less so for IFN-γ production. In contrast, TNF and IL-2 productions were not enhanced by CD28 costimulation in patients' memory $CD4^+$ T cells, although all memory $CD4^+$ T cell express CD28 (Fig. S3 c). Similar experiments performed on $CD8^+$ memory T cells (Fig. 5 b) showed that CD3 stimulation alone induced TNF and IFN-γ production and CD107a surface expression equally in controls and patients. Anti-CD28 Abs

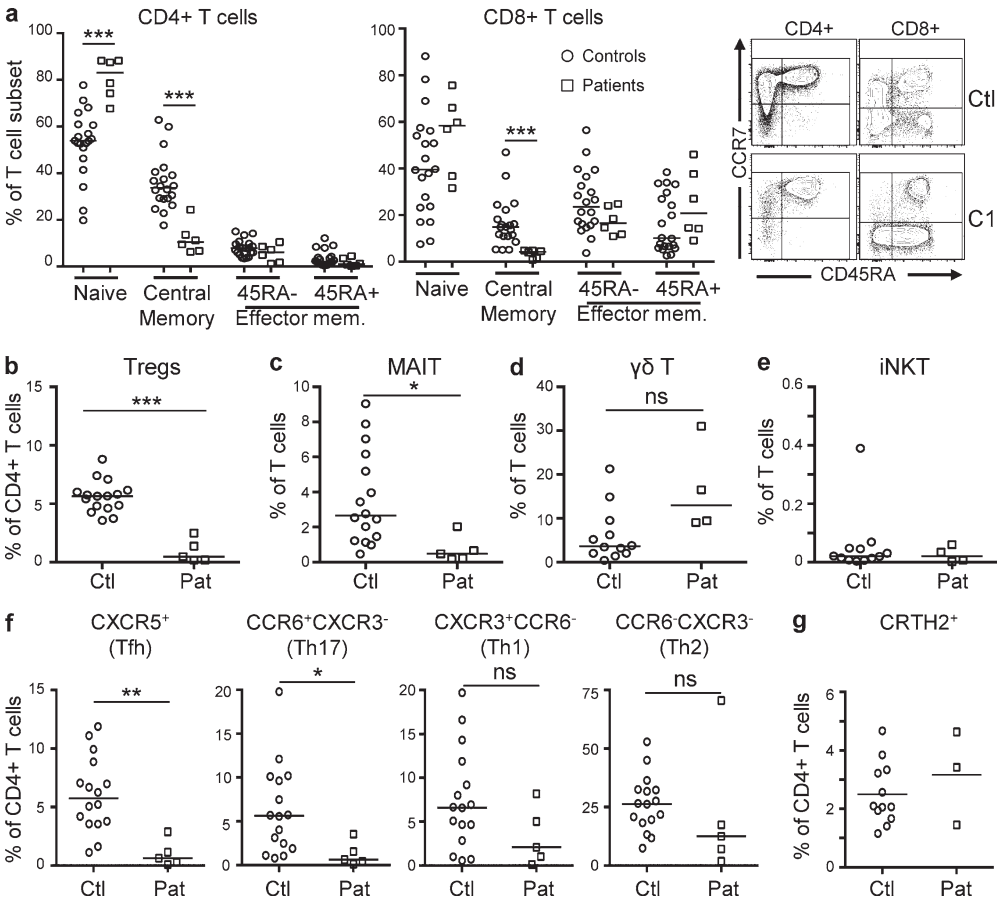

Figure 4. **T cell immunophenotyping of RLTPR-deficient patients.** (a) Frequency of naive (CD45RA$^+$CCR7$^+$), central memory (CD45RA$^-$CCR7$^+$), and effector memory (mem.; CD45RA$^{+/-}$CCR7$^-$) compartments in CD4$^+$ and CD8$^+$ T cells of controls (Ctl) and patients. The horizontal bars represent the median. (Right) Representative FACS plots are depicted. Data show 20 controls and 6 patients. (b) Frequency of T reg cells among CD4$^+$ T cells. Pat, patient. (c–e) Frequencies of MAIT cells (c), γδ T cells (d), and iNKT cells (e) among CD3$^+$ T cells. (b and c) Data show 16 controls and 5 patients. (d and e) Data show 12 controls and 4 patients. (f) Frequency of Th cell subsets in CD4$^+$ T cells. The different markers used to identify Th cell subsets are indicated above the plots. Data show 16 controls and 5 patients. (g) Frequency of CRTH2$^+$ subset in CD4$^+$ T cells. Data show 12 controls and 3 patients. Each symbol corresponds to an individual patient or healthy control. The horizontal bar represents the mean. (a–f) A Mann–Whitney test was used. *, $P < 0.05$; **, $P < 0.01$; ***, $P < 0.001$.

did not enhance any of these responses in controls or patients, suggesting that memory CD8$^+$ T cell do not rely on CD28 co-stimulation for these three readouts, regardless of CD28 expression. This is consistent with a lack of CD28 expression on many memory CD8$^+$ T cells and the potent effector function (cytotoxicity) of CD8$^+$CD28$^-$ T cells that can be induced after TCR engagement (Azuma et al., 1993). Overall, these results suggested that RLTPR plays an essential role in the CD28 co-stimulation pathway in human CD4$^+$ T cells, at least in these experimental conditions.

NF-κB signaling upon CD28 co-stimulation in patients' T cells

The human NF-κB signaling pathway is involved in T cell activation after CD3/CD28 co-stimulation (Thaker et al., 2015). We thus assessed phosphorylation of P65 (the product of the *RELA* gene) by flow cytometry in four patients (A3, B1, B2, and C1) and eight healthy controls upon stimulation of CD4$^+$ and CD8$^+$ PHA-driven T cell blasts with combinations of Abs against CD3, CD28, and/or CD2. In control CD4$^+$ T cells, isolated CD28 cross-linking induced strong P65 phosphorylation, whereas intermediate and weak phosphorylations were observed upon isolated CD3 and CD2 cross-linking, respectively. In controls, CD3 and CD2 co-stimulation induced a strong increase of P65 phosphorylation when compared with CD3 alone, whereas CD3 and CD28 co-stimulation did not markedly increase P65 phosphorylation when compared with CD28 alone. In the patients' CD4$^+$ T cells, P65 phosphorylation was not statistically different from controls upon isolated CD3 or CD2 stimulation or upon CD2 and CD3 co-stimulation. In contrast, there was no P65 phosphorylation upon isolated CD28 stimulation in patients' CD4$^+$ PHA T cells (Fig. 5 c). Moreover, P65 phosphorylation in the patient's CD4$^+$ PHA T cells upon CD3 and CD28 co-stimu-

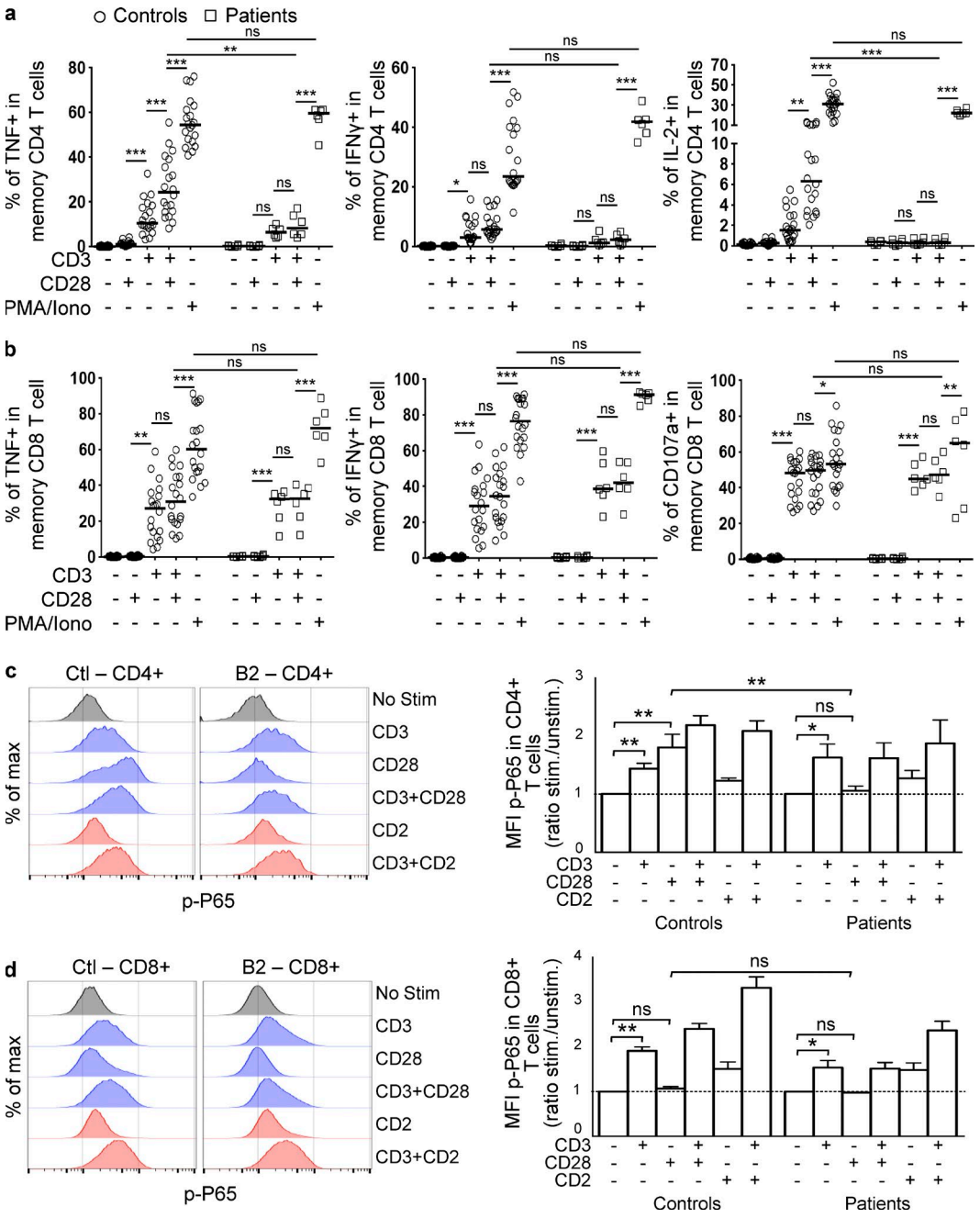

Figure 5. **Impaired CD28 co-stimulation in patients' CD4⁺ T cells.** (a) Frequency of TNF $^{+}$, IFN-γ^{+}, and IL-2^{+} CD4^{+} memory T cells in healthy controls and patients after stimulation with the P815 cell line in the presence of 5 µg/ml anti-CD3 and/or 5 µg/ml anti-CD28 mAbs. 40 ng/ml PMA and 10^{-5} M ionomycin (Iono) stimulation was used as a positive control. One-way ANOVA and Mann–Whitney tests were used. (b) Frequency of TNF^{+}, IFN-γ^{+}, and CD107a^{+} CD8^{+} memory T cells in controls and patients after stimulation with the P815 cell line in the presence of 5 µg/ml anti-CD3 and/or 5 µg/ml anti-CD28 mAbs. 40 ng/ml PMA and 10^{-5} M ionomycin stimulation was used as a positive control. One-way ANOVA and Mann–Whitney tests were used. (a and b) Data show 20 controls and 6 patients. (c and d) Phospho-P65 (p-P65) detection by flow cytometry in CD4^{+} (c) and CD8^{+} (d) PHA blasts after cross-linking of indicated cell surface receptors. Representative FACS plot (left) and recapitulative bar graphs of eight controls (Ctl) and four patients (A3, B1, B2, and C1; right) are shown. The values represent the mean ± SEM. Wilcoxon matched-pairs signed rank test and Mann–Whitney tests were used. *, $P < 0.05$; **, $P < 0.01$; ***, $P < 0.001$. stim, simulated; unstim., unstimulated.

lation was indistinguishable from that after CD3 stimulation alone (Fig. 5 c). In controls' CD8^{+} PHA T cells, CD3 and CD2 cross-linking alone induced intermediate and weak P65 phosphorylation, respectively, whereas CD2 and CD3 co-stimulation synergized for P65 phosphorylation (Fig. 5 d). In contrast with controls' CD4^{+} T cells and in line with cy-

tokine production data (Fig. 5, a and c), CD28 cross-linking alone induced weak/absent P65 phosphorylation in controls' $CD8^+$ PHA T cells, and CD28 did not synergize with CD3 stimulation either (Fig. 5 d). As a consequence, no phenotype could be expected in patient's $CD8^+$ T cells upon CD28 engagement (Fig. 5 b). Altogether, these data demonstrate that RLTPR is required for CD28-mediated activation of NF-κB in human $CD4^+$ T cells.

RLTPR deficiency compromises proliferation of naive but not memory $CD4^+$ T cells

To determine the potential role of RLTPR in CD28 signaling in human T cells, as established for mouse T cells (Liang et al., 2013), we first analyzed in vitro proliferation of naive and memory $CD4^+$ T cells from healthy controls ($n = 5$) and patients ($n = 4$). These cells were sorted, labeled with CFSE, and then cultured under different conditions: anti-CD2/CD3/CD28 beads alone (Th0) or under Th1 (IL-12), Th2 (IL-4), or Th17 (IL-1β, -6, -21, and -23 and TGF-β) polarizing conditions; cell division and cytokine production were determined at different times. Interestingly, after 4 d of culture, we observed reduced proliferation of naive $CD4^+$ T cells from RLTPR-deficient patients, when compared with those from healthy controls under Th0 conditions (Fig. 6 a). Frequency of IL-2^+ cells after culturing patients' naive $CD4^+$ T cells in Th0 conditions was reduced compared with controls, perhaps contributing to their proliferation defect (Fig. 6 b). This indicates that signaling through CD2 cannot completely overcome the CD28 signaling defect in naive $CD4^+$ T cells. In contrast, proliferation of RLTPR-deficient naive $CD4^+$ T cells was restored to normal levels when cultured under Th1 or Th2 but not Th17 conditions, suggesting that cytokines such as IL-12 or IL-4 can overcome the CD28-related defect in RLTPR-deficient $CD4^+$ T cells (Fig. 6 c). In contrast with $CD4^+$ naive T cells, there was no difference in proliferation and frequency of IL-2–producing cells between patients and controls after 4-d culture of memory $CD4^+$ T cells with anti-CD2/CD3/CD28 beads (Th0 conditions; Fig. 6, d and e).

RLTPR regulates expression of prosurvival genes in naive and memory $CD4^+$ T cells

A key function of CD28 signaling is to promote T cell survival via the induction of Bcl-xL (Boise et al., 1995). To determine whether RLTPR mutations affected CD28-mediated up-regulation of key survival proteins, we assessed expression of prosurvival *BCL2L1* (Bcl-xL) and *BCL2* and proapoptotic *BCL2L11* (Bim) mRNA by qRT-PCR in activated naive and memory $CD4^+$ T cells. Whereas no significant difference of *BCL2* expression was detected in both naive and memory RLTPR-deficient $CD4^+$ T cells, we found significantly lower induction of *BCL2L1* in RLTPR-deficient naive (fivefold reduced) and memory (twofold reduced) $CD4^+$ T cells and increased (fourfold) expression of *BCL2L11* in RLTPR-deficient memory $CD4^+$ T cells compared with controls (Fig. 6 f). Thus, RLTPR deficiency potentially compromises survival of activated $CD4^+$ T cells, which might explain the paucity of memory $CD4^+$ T cells in these patients.

RLTPR functions intrinsically to regulate the generation of "Th1" and "Th17" cells but not "Th2" effector $CD4^+$ T cells

To assess the impact of RLTPR deficiency on the function of memory $CD4^+$ T cells, we measured cytokine secretion after culture under Th0 conditions. RLTPR-deficient memory $CD4^+$ T cells exhibited dramatic reductions in production of IFN-γ, TNF, IL-17A/F, and IL-22 (Fig. 6 g), as well as IL-6 and IL-10 (Fig. 6 h). In contrast, secretion of the Th2 cytokines IL-4, IL-5, and IL-13 was unaffected by RLTPR deficiency (Fig. 6 i). To determine whether defects in cytokine secretion by RLTPR-deficient memory $CD4^+$ T cells were intrinsic or extrinsic, we next assessed the ability of patients' naive $CD4^+$ T cells to differentiate into Th1, Th2, or Th17 lineages in vitro under appropriate polarizing conditions (Fig. 6 j). RLTPR-deficient naive $CD4^+$ T cells showed impaired differentiation into IFN-γ/TNF- and IL-17A/IL-17F–producing cells under Th1 and Th17 conditions, fivefold and 10-fold reduction, respectively, compared with controls, as determined by secretion of these cells after 5 d of in vitro culture (Fig. 6 j). In contrast, production of IL-5 and IL-13 under Th2 conditions was only modestly affected (twofold decrease compared with controls; Fig. 6 j). To extend these findings, we determined by qRT-PCR expression of the master regulators of Th1 (*TBX21*, encoding Tbet), Th2 (*GATA3*), and Th17 (*RORC*, encoding RORγt) differentiation in naive $CD4^+$ T cells after in vitro polarization (Fig. 6 k). Surprisingly, induction of *TBX21* and *RORC* expression in RLTPR-deficient naive $CD4^+$ T cells was comparable with that observed for control naive $CD4^+$ T cells. Consistent with the cytokine data, induction of *GATA3* in RLTPR-deficient naive $CD4^+$ T cells was also intact. These data suggest that RLTPR is important for the initial activation and maintenance of naive $CD4^+$ T cells, inasmuch that RLTPR deficiency severely compromises the survival and subsequent differentiation of these cells toward Th1 and Th17, but modestly Th2, fates. Consistent with this interpretation, analysis of the proportion of viable RLTPR-deficient $CD4^+$ T cells expressing Th1 and Th17 cytokines, as determined by intracellular staining, was similar to controls (not depicted), suggesting the reduction in levels of accumulated secreted cytokines during the culture period is caused by impaired cell survival rather than differentiation. Lastly, to further extend our analysis of $CD4^+$ T cell subsets in vitro, we assessed up-regulation of CD40L and inducible T cell co-stimulator (ICOS), two receptors critical for the function of Tfh cells, on naive $CD4^+$ T cells after stimulation with anti-CD2/CD3/CD28 beads (Fig. 6 l). Frequency of CD40L and MFI of ICOS on RLTPR-deficient naive $CD4^+$ T cells were reduced, equating to ∼50% of the levels detected on cells from healthy controls. This underscores our finding of reduced proportions of circulating Tfh-type cells in the peripheral blood of RLTPR-deficient patients and suggests poor $CD4^+$ T cell help for B cell differentiation.

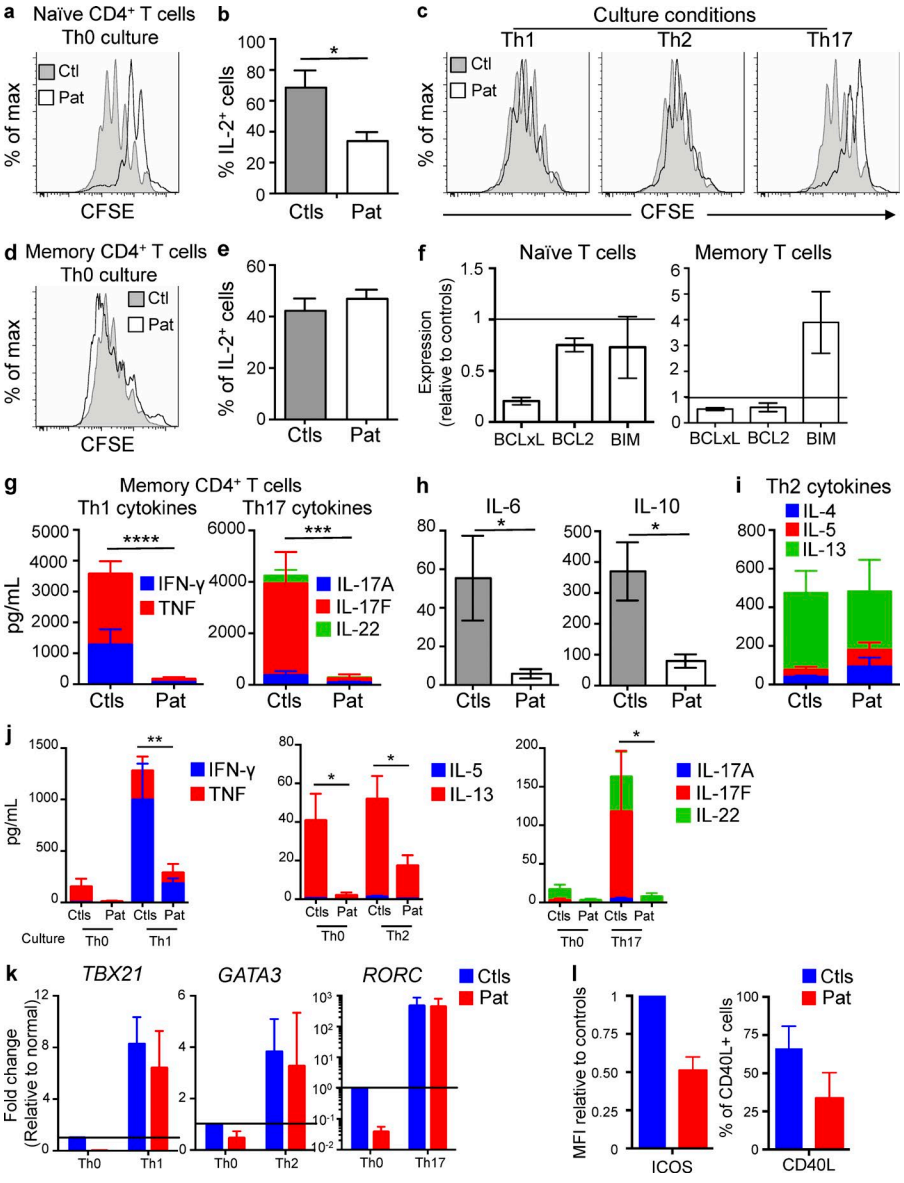

Figure 6. **Proliferation and differentiation of CD4+ Th cells in vitro.** (a) CFSE dilution of naive CD4+ T cells sorted from a representative control (Ctl) and patient (Pat; B2) after 4 d of culture in the presence of CD2/CD3/CD28-coated beads (Th0). (b) Percent IL-2+ naive CD4+ T cells after 4 d of culture under Th0 conditions. Data are mean ± SEM. *, P < 0.05. *n* = 4–5. (c) CFSE dilution of naive CD4+ T cells sorted from a representative control and patient (B2) after 4 d of culture under Th1 (IL-12), Th2 (IL-4), or Th17 (IL-1β, -6, -21, and -23; TGF-β) cell-polarizing conditions. Similar results were obtained when cells from three additional RLPTR-deficient cells were analyzed under the same conditions. (d) CFSE dilution of memory CD4+ T cells sorted from a healthy control or RLTPR-deficient patient (B2) and then cultured for 4 d in the presence of CD2/CD3/CD28-coated beads (Th0). (e) Percent IL-2+ memory CD4+ T cells after 4 d of culture under Th0 conditions. CFSE profiles are representative of data derived from five independent experiments using cells from different donors and patients. Data are mean ± SEM. (f) Expression of *BCL2*, *BCL2L1* (Bcl-xL), and *BCL2L11* (BIM) by activated CD4+ T cells from five controls and four RLTPR-deficient patients, as determined by qRT-PCR. The values represent the mean ± SEM mRNA levels of the indicated gene expressed by naive (left) and memory (right) CD4+ T cells relative to that expressed by corresponding cells from healthy controls (normalized to 1, indicated by the solid horizontal line; *n* = 2–3). (g–i) Secretion of Th1 (TNF and IFN-γ) and Th17 (IL-17A, IL-17F, and IL-22) cytokines (g), IL-6 and IL-10 (h), and Th2 (IL-4, IL-5, and IL-13) cytokines (i) by memory CD4+ T cells after 4 d of culture under Th0 conditions. The values represent the mean ± SEM from independent experiments using cells from five different healthy donors or four patients. *, P < 0.05; ***, P < 0.001; ****, P < 0.0001. *n* = 4–5. (j) Secretion of the indicated Th1 (TNF and IFN-γ), Th2 (IL-5 and IL-13), and Th17 (IL-17A, IL-17F, and IL-22) cytokines by naive CD4+ T cells after 4-d culture under Th1, Th2, or Th17 cell-polarizing conditions. The values represent the mean ± SEM and are derived from independent experiments using cells from five different healthy donors or four patients. *, P < 0.05; **, P < 0.01. (k) Expression of *TBX21* (Tbet), *GATA3*, and RORC (RORγt), as determined by qRT-PCR, by control and RLTPR-deficient naive CD4+ T cells after culture under Th0, Th1, Th2, or Th17 conditions. The values represent the mean ± SEM fold change in expression relative to naive CD4+ T cells from healthy controls cultured under Th0 conditions (*n* = 2–3). (l) CD40L frequency and ICOS MFI on sorted naive CD4+ T cells from four patients and three controls after 4 d of culture under Th0 conditions. MFI was normalized to controls' MFI. Two-way ANOVA was applied for g, l, and j. A Mann–Whitney test was applied for h.

Memory B cell deficiency in RLTPR-deficient individuals

RLTPR-deficient patients have a T cell deficiency and an Ab-related infectious phenotype, including bacterial infections of the respiratory tract. Furthermore, RLTPR is strongly expressed in B cells (Fig. 3 h). For these reasons, we first evaluated whether RLTPR deficiency could affect B cell development or function. B cell counts were normal in all patients except B1 who showed a slight decrease. Among all B cell subsets analyzed ex vivo, proportions of transitional B cells ($CD10^+$) were normal, whereas there was a decrease in all memory ($CD27^+$) B cells and IgG^+ B cells (Table 2 and Fig. 7, a and b). Serum Ig isotypes levels were determined in all patients, including B1 who was then on IVIG replacement therapy. IgM levels were elevated in all patients except C1. IgG

Table 2. **Patients' B cell immunophenotyping**

	Units	A1	C1	Normal range	B1	B2	Normal range
		17 yr	18 yr		25 yr	24 yr	
Number of lymphocytes	/µl	6,700	5,371		2,000	2,600	
B lymphocyte							
$CD19^+$	%	5	15	6–23	4	8	6–17
$CD19^+$	/µl	335	806	110–570	80	208	92–420
$CD27^+/CD19^+$	%	0.9	1	7–29	7	54	>12.6
$CD27\text{-}IgD^+/CD19^+$	%	98.3	94	61–87	90	47	>67.5
$CD27^+IgD^+/CD19^+$	%	0.4	0.4	2.6–13.4	6	47	nt
$CD27^+IgD^-/CD19^+$	%	0.4	0.9	4–21.2	2	5	>6.5
$CD27^-IgD^-/CD19^+$	%	0.9	nt	1.4–13	3	0.9	nt
CD21 LOW/$CD19^+$	%	42	nt	nt	2	19	nt
$CD38^{++}M^{++}$CD21 LOW/$CD19^+$	%	1	nt	nt	0.2	nt	nt
$CD21^{++}CD24^+/CD19^+$	%	93	nt	nt	91	98	nt
$CD21^+CD24^{++}/CD19^+$	%	3	nt	nt	5	0.3	nt
$CD21^-CD24^-/CD19^+$	%	1	nt	nt	1	1.3	nt
$CD38^{++}IgM^{++}/CD19^+$	%	nt	nt	nt	6	nt	nt

nt, not tested.

levels were above normal for B1, B2, and C1 and normal in the other patients. IgA levels were elevated in A2, A3, and B1 and normal for the other patients. Serum IgE levels were high in B1, particularly during teenage years (Table 3 and Table S5). Antigen-specific Abs to bacterial vaccines were undetectable in B1 and B2, including when tested after diphtheria, tetanus, and pertussis vaccination recall for B1 (Table 3). B1 had Abs against pneumococcal capsular glycans, and all patients have detectable viral-specific Abs (Table 3 and Table S1). Despite the absence of clinical signs of autoimmunity, some auto-Abs were detectable in the patients (especially in B2), but none of them were directed against IL-17 or IFNs (Fig. 7 d and Fig. S4). Altogether, these data suggested that RLTPR-deficient patients displayed a deficiency of memory B cells coupled to an Ab deficiency against some but not all antigens.

Defective NF-κB activation downstream B cell receptor (BCR) in RLTPR-deficient individuals

These data prompted us to test whether there could be a B cell–intrinsic defect. Using phospho-flow cytometry on primary $CD20^+$ B cells, we assessed NF-κB (degradation of IκBα and phosphorylation of P65) and mitogen-activated protein kinase (phosphorylation of ERK1/2) activation in response to BCR stimulation with either anti-IgM Abs or CD40 stimulation with pentameric CD40L (Fig. 7, c–e). All patients' and control B cells responded strongly to PMA for the three readouts tested, indicating that RLTPR deficiency does not cause a general impairment in the ability of patient B cells to respond to exogenous stimuli. B cells from three RLTPR-deficient patients also showed a strong and normal NF-κB activation upon CD40 stimulation. Interestingly, although anti-IgM Abs induced NF-κB activation in controls, BCR engagement of RLTPR-deficient B cells failed to induce IκBα degradation or phosphorylation of P65. ERK1/2 phosphorylation upon IgM cross-linking was maintained in patients' B cells, albeit slightly diminished in two of the three patients, indicating that the BCR-responsive pathway was not fully abrogated in the absence of RLTPR. These data show that RLTPR-deficient B cells have a partially defective signaling pathway, at least via NF-κB, but an intact CD40 signaling pathway, at least for the readouts tested. Beyond B cells and T cells, we also found decreased production of IFN-γ by NK and T cells upon bacille Calmette–Guérin (BCG) plus IL-12 activation of whole blood from patients (Feinberg et al., 2004) and normal IL-10 and IL-6 production by monocytes upon activation by TNF and microbial products, respectively (Fig. S5, a and b; Foey et al., 1998). Altogether, our results indicate that six patients from three kindreds with AR complete RLTPR deficiency display at least T cell– and B cell–intrinsic anomalies, accounting for the diversity and severity of their infectious phenotype.

DISCUSSION

Here, we report six patients from three unrelated kindreds from three different ethnicities (Morocco, Tunisia, and Turkey) with an AR form of complete functional RLTPR deficiency. Our study indicates that RLTPR is necessary for the development of T reg cells and MAIT cells and the maturation of naive $CD4^+$ T cells into memory cells, as well as their differentiation into Th1, Th17, and Tfh cells. The underlying mechanism probably involves impaired NK-κB signaling downstream of CD28, as inferred from the abolished P65 phosphorylation in patients' $CD4^+$ T cells. Intriguingly, NF-κB activation was also impaired in patients' B cells after BCR but not CD40 ligation, suggesting an important role for RLTPR in antigen-receptor signaling in B cells. A shared mechanism in T and B cells may involve the disruption of the CARMA1–RLTPR interaction (Roncagalli et al., 2016). In addition, our finding of reduced proportions of circulating Tfh-type cells in the peripheral blood of RLTPR-deficient patients, together with diminished

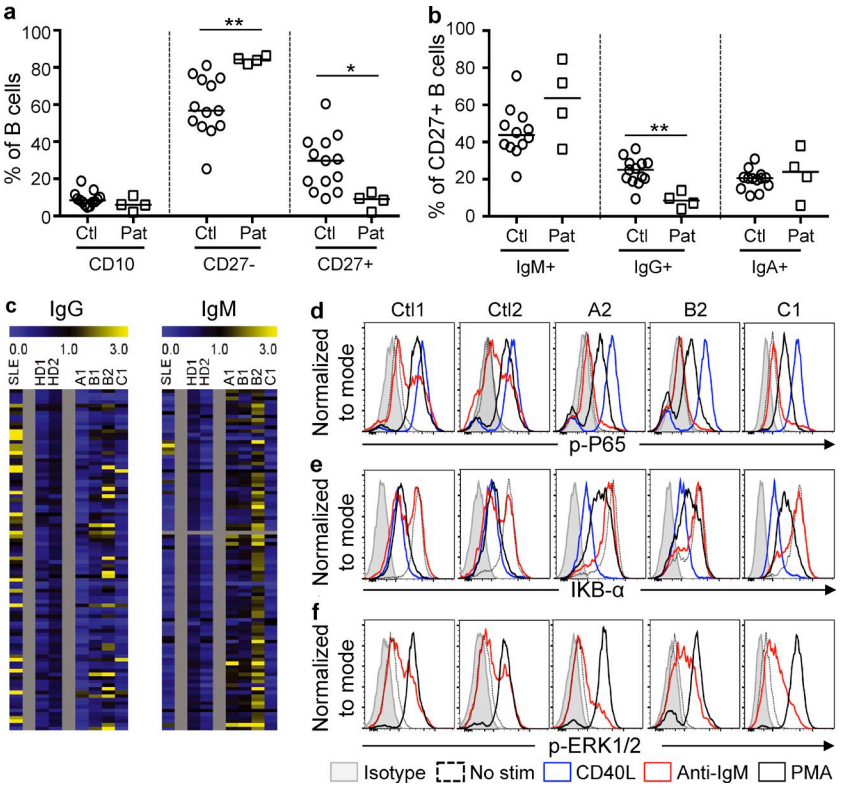

Figure 7. **B cell immunophenotyping and impaired NF-κB activation downstream the BCR of RLTPR-deficient patients.** (a) Frequencies of transitional ($CD10^+CD27^-$), naive ($CD10^-CD27^-$), and memory ($CD10^-CD27^+$) B cells among $CD19^+$ B cells. A Mann–Whitney test was used. Data show 13 controls and 4 patients. Ctl, control; Pat, patient. (b) Frequency of IgM^+, IgG^+, and IgA^+ cells within the memory B cell subset. Each symbol corresponds to an individual patient or healthy control. The horizontal bar represents the mean. A Mann–Whitney test was used. *, $P < 0.05$; **, $P < 0.01$. Data show 12 controls and 4 patients. (c) Heat map of IgG and IgM serum auto-Abs to 94 self-antigens in four RLTPR-mutated patients (A1, B1, B2, and C1) and in two healthy donors (HD) and one patient with systemic lupus erythematosus (SLE) who served as negative and positive controls, respectively. Each line represents a different self-antigen. For each self-antigen, a colorimetric representation of RAR in each sample is shown according to the scale depicted at the top. (d and e) Phosphorylation of P65 (d) and degradation of IκBα (e) after stimulation of controls' and patients' PBMCs with CD40L (blue line), anti-IgM (red line), or PMA (black line). (f) Phosphorylation of ERK1/2 (pERK) after stimulation of controls' and patients' PBMCs with anti-IgM (red line) or PMA (black line). No stim, no stimulation.

expression of CD40L and ICOS on activated RLTPR-deficient naive $CD4^+$ T cells, predicts numerical and functional defects in Tfh cells in the absence of RLTPR. Thus, the B cell phenotype of impaired Ab responses in vivo and in vitro and low memory B cells probably results from both B cell–intrinsic and B cell–extrinsic defects, namely poor BCR-mediated activation and a concomitant deficit of Tfh cells. These defects may collectively account for the poor Ab responses to vaccinations and some of the recurrent bacterial infections of RLTPR-deficient patients. In contrast to B cells and $CD4^+$ T cells, RLTPR deficiency had only a modest effect, if any, on the development of $CD8^+$ T cells, γδ T cells, and iNKT cells. The immunological similarities between RLTPR-deficient humans and Rltpr-mutant ($Rltpr^{bas}$) mice, as reported in previous and the companion paper, are striking (Liang et al., 2013; Roncagalli et al., 2016). First of all, as in two of the three kindreds, the deleterious $Rltpr^{bas}$ mutation in mice affects a highly conserved leucine in the LRR. Moreover, $Rltpr^{bas}$ mice display a profound reduction of circulating T reg cells and memory $CD4^+$ T cells (Roncagalli et al., 2016). The CD3/CD28 co-stimulation was also abolished in $Rltpr^{bas}$ mice in terms of proliferation and cytokine production by $CD4^+$ T cells. Likewise, the CD3 and CD2 co-stimulation is also intact in RLTPR-deficient mouse $CD4^+$ T cells. In mice, in contrast to $CD4^+$ T cells, CD28 co-stimulation had a modest impact on the CD3/CD28-induced proliferation of mouse $CD8^+$ T cells (Liang et al., 2013). We could not document such impact in humans because control $CD8^+$ T cells did not respond to CD28 stimulation in our experimental settings. Conversely, mouse B cells do not seem to display any detectable cell-intrinsic phenotype, perhaps reflecting differences between both species (Liang et al., 2013; Roncagalli et al., 2016).

Table 3. **Immunoglobulins**

	Age	IgG	IgA	IgM	IgE	IgG1	IgG2	IgG3	IgG4
	yr	*g/L*	*g/L*	*g/L*	*kU/L*	*g/L*	*g/L*	*g/L*	*g/L*
Normal range	>10	6.65–12.78	0.7–3.44	0.5–2.09	<114	>4	>0.6	>0.17	
	2	4.82–8.96	0.33–1.22	0.5–1.53	<40.3	>4	<0.3	>0.13	
A1	17	8.27	2.48	3.62	<5	6.9	3.15	0.83	0.003
A2	2	7.01	2.32	3.06	<2	4.5	3.57	0.61	0.003
A3	2	6.38	1.32	1.87	<2	4.8	1.22	0.49	0.004
B1	26	16.89	3.87	3.82	2,158	9.2	3.5	0.91	0.06
B2	24	12.56	2.4	3.44	2.3	7	2.24	0.93	0.013
C1	17	13.52	1.32	1.67	35.2	8.1	2.45	1.14	0.22

It is intriguing that clinical signs of autoimmunity do not accompany the strong decrease of Foxp3$^+$ T reg cells in the patients (0–2.5% of CD4$^+$ T cells for a normal range between 5 and 10%). Interestingly, all patients tested had a variety of auto-Abs, and one of them (B1) had a facial eruption reminiscent of lupus, suggesting that currently covert autoimmunity might flare up later in life. B1 and B2, homozygous for a nonsense mutation encoding a truncated protein, have more auto-Abs than the other patients, which perhaps not coincidentally are homozygous for missense mutations. Clearly, however, the patients do not have even remotely the life-threatening autoimmune phenotype seen in patients with other inborn errors of T reg cells, such as IPEX (immunodysregulation polyendocrinopathy enteropathy X-linked) syndrome caused by *FOXP3* mutations (Bennett et al., 2001; Wildin et al., 2001) or patients with mutations in *LRBA* or *CTLA4* that also impair T reg cell function or numbers and are associated with autoimmunity (Kuehn et al., 2014; Alkhairy et al., 2016). RLTPR-deficient patients do not even display the common autoimmune manifestations seen in most types of CID (Notarangelo, 2014; Alkhairy et al., 2016). A plausible hypothesis to account for the paradoxical lack of clinical autoimmunity is that the diminution of T reg cells is compensated by the lack of CD28 activation of effector CD4$^+$ T cells, poor generation, maintenance or expansion of memory CD4$^+$ T cells, and impaired survival of memory CD4$^+$ T cells because of compromised CD28-mediated induction of Bcl-xL. Consistently, a lack of autoimmune manifestations despite low T reg cells has also been reported in patients with CARD11 and BCL10 deficiencies (Greil et al., 2013; Stepensky et al., 2013; Torres et al., 2014; Pérez de Diego et al., 2015). As in RLTPR-deficient patients, T cells from these patients fail to respond to CD3 plus CD28 co-stimulation and present a predominant naive phenotype (Stepensky et al., 2013; Pérez de Diego et al., 2015). MALT1-deficient T cells do not respond to CD28 co-stimulation either, but these patients have normal counts of T reg cells (Jabara et al., 2013; McKinnon et al., 2014; Pérez de Diego et al., 2015; Punwani et al., 2015). One may further speculate that the emergence of the CD28 co-stimulation pathway rendered T reg cells necessary. The clinical contrast between AR RLTPR deficiency and autosomal dominant CTLA4 deficiency, which manifests as a severe autoimmunity (Kuehn et al., 2014; Schubert et al., 2014), neatly illustrates the respective roles of the CD28 and CTLA4 pathways in humans. Mice lacking RLTPR do not seemingly develop any spontaneous autoimmune manifestations (Roncagalli et al., 2016). Likewise, mice lacking CD28 have reduced T reg cell numbers and are also protected from various T cell–mediated experimental autoimmune diseases (Shi et al., 1998; Chang et al., 1999; Tada et al., 1999; Zhang et al., 2013). In addition, T reg cell–specific conditional CD28 knockout mice have low numbers of T reg cells, and the accumulation of activated T cells underlies severe autoimmune diseases (Zhang et al., 2013).

A striking feature of RLTPR-deficient patients is their bronchopulmonary and cutaneous allergy, which is reminiscent of patients with hyper-IgE syndrome, such as DOCK8 deficiency (Zhang et al., 2009, 2016; Aydin et al., 2015). The skin appearance is striking (Fig. S1). The histology of the skin lesions is consistent with severe eczema, with a lymphocytic infiltrate. Others lesions resemble psoriasis, which is probably a consequence of chronic eczema. These lesions mostly contain CD8$^+$ T cells, some macrophages, and fewer mastocytes. The study of the patients' Th cell differentiation ex vivo and in vitro provides an explanation for this phenotype. Specifically, RLTPR-deficient CD4$^+$ T cells have normal production of Th2 cytokines but impaired production of Th1 and Th17 effector cytokines. This suggests that the CD28–RLTPR–CARD11 pathway is necessary for the development of Th1, Th17, and Tfh cell subsets and that the primordial, original differentiation pathway of CD4$^+$ T cells, by default, is along the Th2 cell pathway. This is observed in many inborn errors of T cells. For example, T cells from patients with loss-of-function mutations in *DOCK8*, *RORC*, *STAT3*, *IL21R*, *IL12RB1*, or *IFNGR1* are biased toward Th2 cells (Ma et al., 2015; Okada et al., 2015; Tangye et al., 2016). Finally, quantitative defects of T cells also result in a Th2 cell bias, as exemplified by Omenn's syndrome (Milner et al., 2007; Ozcan et al., 2008). Patients with CARD11, BCL10, and MALT1 deficiencies were not reported to develop allergy or a Th2-biased T cell compartment. Similar absences of a Th2 cell bias were observed in mice with complete BCL10 and CARD11 deficiency (Ruland et al., 2001; Hara et al., 2003; Medoff et al., 2006). However mice carrying hypomorphic CARD11 mutations, which do not completely abrogate CD3/CD28-induced NF-κB activation, present a strong Th2 cell bias, elevated-IgE, dermatitis, and low T reg cells (Altin et al., 2011), a phenotype reminiscent of human RLTPR deficiency. However, in contrast to the RLTPR-deficient patients, Rltpr^{bas} mice do not display a skin/fur phenotype (Liang et al., 2013). However, the mice were not tested for allergy in experimental conditions.

The poor maturation of CD4$^+$ T cells into memory cells and Th1, Th17, and Tfh cell subsets explains some of the patients' infectious phenotypes. Mycobacterial disease probably results from poor IFN-γ production by Th1 cells (Bustamante et al., 2014) and pyogenic bacterial infections from the poor Ab response and impaired development of Tfh cells, with or without B cell–intrinsic anomalies in the BCR responsive pathway (Tangye et al., 2013). The pathogenesis of staphylococcal disease is less clear, as no T cell cytokine or membrane-bound molecule has been unambiguously incriminated for now. Impaired production of or response to IL-6 by T cells might be involved, as suggested by the development of staphylococcal disease in patients with impaired IL-6 responses or auto-Abs to IL-6 (Puel et al., 2008; Kreins et al., 2015). Consistent with this, we noted dramatically reduced production of IL-6 by RLTPR-deficient memory CD4$^+$ T cells in vitro. Impaired Th17 cell immunity is probably also involved in pe-

Table 4. **Vaccine serology**

	Date	Antitetanus IgG	Antidiphtheric IgG	Antipneumococcal IgG
B1	01/06/07	0.03 UI/ml[a]	0.01 UI/ml[a]	ΔOD = 2.7
	27/06/07	<0.1 KUI/L[b]	<0.1 KUI/L[b]	25 µg /ml
	12/10/07	<0.01 UI/ml[a]	0.03 UI/ml[a]	ΔOD = 2.5
B2	25/02/15	<0.1 UI/ml	<0.1 UI/ml	nt

Antipneumococcal IgG: positive >0.3 µg/ml or ΔOD >1.2. nt, not tested.
[a]Protection limit: ≥0.01 UI/ml
[b]Protection limit: ≥0.6 KUI/l

ripheral staphylococcal disease (Puel et al., 2012). Similarly, mucocutaneous candidiasis is most likely the consequence of impaired Th17 cell development (Puel et al., 2012). In humans with DOCK8 deficiency, the Th17 cell subset is also abnormal, accounting for the presence of similar infections, including candidiasis and staphylococcal disease (Keles et al., 2016; Tangye et al., 2016). It may not be coincidental that DOCK8 appears to be a partner of RLTPR in biochemical studies reported in the companion paper (Roncagalli et al., 2016). However, patients with DOCK8 deficiency have a variety of viral diseases of the skin not seen in RLTPR deficiency, probably because of structural anomalies of their T cells (Zhang et al., 2009, 2016). Although our patients did not display unusually severe viral illnesses, detection of EBV viremia in four of the six patients suggests that they may be prone to EBV-driven clinical manifestations later in life. Patients with deficiency of CD27, another T cell co-stimulatory molecule, were specifically vulnerable to EBV (van Montfrans et al., 2012; Salzer et al., 2013; Alkhairy et al., 2015). In contrast, a patient with OX40 deficiency, another T cell co-stimulatory molecule, was specifically vulnerable to HHV8 infection (Byun et al., 2013). RLTPR-deficient mice were not challenged with infectious agents and do not develop infections spontaneously (Roncagalli et al., 2016). Although CD28-deficient mice are vulnerable to some bacteria, such *Salmonella typhimurium* and *Listeria monocytogenes* (Mittrücker et al., 1999, 2001), they are normally resistant to most pathogens (Shahinian et al., 1993; Hogan et al., 2001; Padigel et al., 2001; Montagnoli et al., 2002). As such, CD28 co-stimulation deficiency alone is unlikely to explain all infections seen in the patients, in line with the observed partial BCR signaling defect. One may speculate that human RLTPR deficiency may affect CARMA1-dependent NF-κB activation in other leukocytes populations, such as DCs and NK cells. Overall, this experiment of nature highlights the nonredundant role of human RLTPR-dependent CD28 co-stimulation with CD3 in T cells and BCR activation of NF-κB in B cells for protective immunity against a variety of infectious agents.

MATERIALS AND METHODS

Case studies

Patient 1 (A1), patient 2 (A2), and patient 3 (A3) are born from a consanguineous Moroccan family. Their parents are first-degree cousins. A2 and A3 are dizygotic twins. Their parents and older sister were healthy. A1 was born without complication and with normal skin. At 2 mo of age, A1 began presenting scaling of scalp (Fig. S1). At the age of 1 yr, he developed scaly erythroderma made of white and thin scales. Skin lesions are itching and evolved by flares, and the linearity of the palms is increased. A focal alopecia has been observed, probably secondary to infections or trauma. At 5 yr old, A1 developed fungal infections of almost all nails of fingers and toes with perionyxis. On his soles, there are pustular-like inflammatory and scaly confluent lesions. In contrast, there are no cutaneous abscesses. He had normal hair, teeth, and sweating. At 8 yr old, A1 was diagnosed with multifocal tuberculosis, involving cervical lymph node, lung, and intestines. The x-ray pictures demonstrated multifocal tuberculosis affecting lung (retrocardiac fireplace and large bilateral hilum) and intestines (intestinal thickening and lymphadenopathy). In total, he received 7 mo of antimycobacterial treatment: 5 mo of streptomycin, isoniazid, rifampin, and pyrazinamide and two months of rifampin and isoniazid, which was a good clinical evolution. In brief, T, B, and NK lymphocytes are normal, as well as respiratory burst on EBV-B cells. Production of IFN-γ and IL-12p40 by whole blood activation was decreased or similar to the healthy controls, respectively (Fig. S5). A1 presented viral meningoencephalitis that was treated by Acyclovir when he was 9 yr old. Viral serology analysis shows that he never encountered HSV-2 (Tables S1 and S2). At 9 yr old, A1 suffered purulent otitis. He had severe dysphagia since the age of 15.5 yr old, caused by peptic stenosis of the lower third of the esophagus secondary to gastroesophageal reflux. He had recurrent bronchitis. A1 has profound anemia, ankyloglossia, and bald tongue. He developed extreme weight loss, which led to cachexia with growth retardation in his life. He was 16.2 kg and 127 cm when he was 17 yr old. Stabilization at −3 SD for weight and −4 SD for height were observed. In 2015, A1 was hospitalized with dyspnea and thoracic pain and died after a rapid deterioration of his general condition with worsening respiratory distress, without tachycardia or gallop rhythm and crackles abdominal defense. A1 was vaccinated according to the Moroccan national immunization program. All the immunological explorations performed for A1 are summarized in Tables 2, 3, 4 and Tables S1, S2, S3, S4, and S5.

A2 was born without noticeable complication. She developed persistent diaper dermatitis since 1 yr old. She has chronic mucocutaneous candidiasis manifested by recurrent

oral thrush and onychomycosis on all fingers and toes since 1 yr old as well as erythematous pruriginous lesions spread on trunk, arm, and legs (Fig. S2). She has recurrent bacterial lung infections and a bronchoalveolar bilateral syndrome (x ray). When she was 21 mo old, she was hospitalized during 10 d for a bacterial lung infection cured after 1-wk treatment with amoxicillin, macrolide, and corticoids. She is currently 2 yr old and is undergoing antibiotic treatment for her recurrent bacterial lung infection (amoxicillin) and fungal infection (fluconazole).

A3 was born without noticeable complications. Although presenting with a less severe overall phenotype than her dizygotic twin sister (A2), A3 also has chronic mucocutaneous candidiasis manifested by an oral thrush and onychomycosis. She does not present obvious skin lesions but persistent diaper dermatitis like her twin sister. She has sibilant rhonchus and a bronchoalveolar bilateral syndrome (x ray). She is currently 2 yr old and is undergoing antibiotic treatment for her recurrent bacterial lung infection (amoxicillin) and fungal infection (fluconazole).

Patient 4 (B1) and her sister (B2) were born to second-degree cousins' parents originating from Tunisia. B1 was born in 1989, and B2 was born in 1990. Their parents and two brothers were healthy. However, their paternal grandfather developed eczema. The skin of both patients was normal at birth. B1 was diagnosed with severe eczema at 1 mo of age, with oozing lesions around the ears, axillary folds, inguinal folds, face, and armpits. She is allergic to yolk egg and peanut. She had cold urticaria and was hospitalized several times. She developed recurrent bronchitis since 1 yr old. Meanwhile, she had nasal obstruction and otitis requiring auripuncture. Since 1995, B1 had asthma and was treated with Fluticasone and Montelukast. Moreover, she had bronchiectasia. Around 10 yr old, she had extensive *Molluscum contagiosium* eruption that was surgically drained. B1 was infected by staphylococcus, resulting in cold subcutaneous abscesses without fever, initially on the scalp and then disseminated on the body, with new lesions every month since the age of 15. Abscesses were drained surgically (on right elbow, left thigh, right buttock, and scalp). B1 developed lupus-like facial erythema (on cheeks, nose, and chin) with cheilitis and several hypo- and hyperpigmented lesions, with atrophic and ulcerative scars on elbows, hips, and legs. She had normal palms, soles, hair, teeth, nails, and sweating. In addition, there were pigmented plaques on her back. Gastric endoscopy allowed us to highlight infection by *Helicobacter pylori*, and then she treated by iron. This patient was under the treatment of Amoxicillin often, also with calcium and since 2008 IVIG at 40 g/kg. When diphtheria, tetanus, and pertussis vaccination was practiced in 2005, she lacked response to protein antigens because she had no antidiphtheria and antitetanus Abs. She had Abs against pneumococcal capsular glycans after unconjugated pneumo23 vaccination (Pasteur vaccine). During her hospitalization, she was vaccinated in a primary vaccination (two injections in 1 mo) to determine whether she responded to these antigens. She is now 27 yr old.

B2 developed erythematous plaques on the face and limbs at 5 yr old. Her skin was dry and itching (8/10), leading to scratching lesions. She had asthma and was treated with steroids (inhalation). B2 also developed bronchiectasia-like B1. She had sun intolerance and was treated by hydroxychloroquine since 5 yr old. Her itching condition improved around 10 yr old, but then, she developed multiple subcutaneous abscesses (five) on her back, right popliteal space, and right thigh. Abscesses were painful with edema and fever at 39°C with shivers, requiring draining in the hospital. Then, she received ambulatory treatment included drains, gauze tents, and oral antibiotics for 7 d. Upon examination, B2 developed large inflammatory and ulcerative plaques in the left armpit and in gluteal folds. She also had numerous psoriasis guttata-like white papules of small size disseminated over the sides, abdomen, and pelvis. Histological data on a cutaneous biopsy showed some areas of subacute eczema and some psoriasis (Fig. S2). Recently, she developed red and scaly lesions of the inguinal folds, which became erosive, red, oozing, and very itchy. These lesions improved with cutaneous steroids and vitamin D treatment. She also had mild ichthyosis predominant on legs. At 6 yr old, she presented pneumonia requiring antibiotics. Epicutaneous allergic tests were negative. Her hair, teeth, nails, and sweating were normal. She is now 26 yr old. All the immunological explorations performed for B1 and B2 are summarized in Tables 2, 3, and 4 and Tables S1, S2, S3, S4, and S5. Exome sequencing data of B2 showing all rare (MAF <0.01) homozygous nonsynonymous coding variants are provided in Table S6.

Patient 6 (C1) was born in 1997 from a nonconsanguineous Turkish family. His parents and younger brother are healthy. In contrast, his two elder brothers had died because of septicemia at 21 (born in 1989) and 12 (born in 1991) yr of age. He was healthy until 2006, except seborrheic dermatitis which was on his scalp and eyebrow, but unresponsive to therapy (Fig. S1). He was admitted to the hospital with fever, weight lost, sweating, and malaise, which had been begun 2 mo ago. He was diagnosed with upper respiratory tract infections and anemia and received various antibiotics. Chest x ray and computed tomography of chest and abdomen revealed multiple lymphadenopathies (the biggest one was 1 × 1 cm in size) at hilum and abdomen, splenomegaly, bilateral miliary nodules distributed to whole lung, consolidation at superior segment of the right lower lobe, pleural effusion, and thickening on the right lung. Tuberculin-purified protein derivative on a skin test was negative and cranial MRI was normal. Lymphoma was excluded, and he was diagnosed as possible miliary tuberculosis, not proven microbiologically. He was treated with four drug antituberculous (isoniazid, rifampicin, pyrazinamide, and streptomycin) for 1 yr with good clinical resolution. Production of IFN-γ and IL-12p40 by whole blood activation are decreased and similar to the healthy controls, respectively (Fig. S6). He developed mumps and varicella infections without complications. He had been vaccinated up to Turkish national vaccination schedule (BCG,

TDaP, Hib, polio vaccine, measles, and hepatitis B) without complications. He had two BCG scars. All the immunological explorations performed are summarized in Tables 2, 3, and 4 and Tables S1, S2, S3, S4, and S5. C1 is 19 yr old now, and he is doing well without treatment.

The experiments described here were conducted in accordance with local, national, and international regulations and were approved by the French Ethics committee, French National Agency for Medicines and Health Products Safety, and by the French Ministry of Research. Informed consent was obtained from all patients or their families, in the case of minors, in accordance with the World Medical Association, the Helsinki Declaration, and European Union directives.

Linkage analysis and WES

We extracted genomic DNA from cell lines or blood samples from patients, their parents, and siblings using the iPrep PureLink gDNA Blood kit and the iPrep instruments from Thermo Fisher Scientific. Multipoint LOD scores were calculated with MERLIN software, assuming that the gene responsible for the defect was AR and displayed full penetrance. WES was performed for A1, B2, and C1. Exome capture was performed with the SureSelect Human All Exon 50 Mb kit (Agilent Technologies). Paired-end sequencing was performed on a HiSeq 2000 sequencing system (Illumina) generating 100-base reads. We aligned the sequences with the GRCh39 reference build of the human genome using the Burrows-Wheeler aligner (Li and Durbin, 2010). Downstream processing and variant calling were performed with the Genome Analysis Toolkit (McKenna et al., 2010), SAMtools (Li et al., 2009), and Picard. Substitution and InDel calls were made with the GATK Unified Genotyper. All variants were annotated using an annotation software system that was developed in house (Ng and Henikoff, 2001; Adzhubei et al., 2010; Kircher et al., 2014).

Genetics

A genomic measure of individual homozygosity was plotted for C1, 19 Middle Eastern individuals from consanguineous families, 8 individuals from families with unknown consanguinity, and 8 individuals from nonconsanguineous families from our in-house WES database. Homozygosity was computed as the proportion of the autosomal genome belonging to runs of homozygosity. The runs of homozygosity were defined as ranging at least 1 Mb of length and containing at least 100 SNPs and were estimated using the PLINK software (Purcell et al., 2007). The centromeres were excluded because they are long genomic stretches devoid of SNPs and their inclusion might inflate estimates of homozygosity if both flanking SNPs are homozygous. The length of the autosomal genome was fixed at 2,673,768 kb as previously described (McQuillan et al., 2008). We estimated the selective pressure acting on RLTPR to be 0.488 (indicative of purifying selection; Fig. S2 e) by estimating the neutrality index (Stoletzki and Eyre-Walker, 2011) at the population level (PN/PS)/(DN/DS), where PN and PS are the number of nonsynonymous and synonymous alleles, respectively, at population level (1000 Genomes Project) and DN and DS are the number of nonsynonymous and synonymous fixed sites, respectively, for the coding sequence of RLTPR.

Cell culture

PBMCs were isolated by Ficoll-Hypaque density centrifugation (GE Healthcare) from cytopheresis or whole-blood samples obtained from healthy volunteers or patients, respectively. PBMCs, PHA blasts, and EBV-B cells were cultured in RPMI medium supplemented with 10% FCS (referred to subsequently as complete medium). PHA blasts were obtained after culturing PBMCs at 2×10^6 cells/ml concentration with 1 µg/ml PHA. After 24-h culture, 10 ng/ml rIL-2 (Thermo Fisher Scientific) was added to the medium. Subsequently, medium and IL-2 were renewed every 48 h. PBMCs were transformed with *H. saimiri* strain C488, as previously described, to ensure continuous growth (Fleckenstein and Ensser, 2004). Saimiri-transformed cells were cultivated in Panserin/RPMI 1640 (ratio 1:1) supplemented with 10% FBS, L-glutamine, gentamycin (1×), and 10 ng/ml human rIL-2 (Thermo Fisher Scientific). All cell culture was performed at 37°C under an atmosphere containing 5% CO_2.

Sanger sequencing

The mutations of *RLTPR* were amplified by PCR performed on genomic DNA. The primers sequences used for the genomic coding region of *RLTPR* are as follows: L372R mutation: forward primer, 5′-CGTCCTAACGTACTGTCGTTCCGGAATCTCGCAGGCACCGACACT-3′ and reverse primer, 5′-AGTGTCGGTGCCTGCGAGATTCCGGAACGACAGTACGTTAGGACG-3′; L525Q mutation: forward primer, 5′-CGCAGGCGCTGTGAGCTCCCAGGATCTGGCGGATAACGGCTTC-3′ and reverse primer, 5′-GAAGCCGTTATCCGCCAGATCCTGGGAGCTCACAGCGCCTGCG-3′; and Q853X mutation: forward mutation, 5′-CCTCCCGGAGCTGCTCCCAGAGTAGCTGCTGCAAGATGCCTTC-3′ and reverse primer, 5′-GAAGGCATCTTGCAGCAGCTACTCTGGGAGCAGCTCCGGGAGG-3′. PCR was performed with Taq polymerase (Invitrogen), using a GeneAmp PCR system (9700; Applied Biosystems). The PCR products were purified by centrifugation through Sephadex G-50 Superfine resin (GE Healthcare) and sequenced with the BigDye Terminator Cycle Sequencing kit (Applied Biosystems). Sequencing products were purified by centrifugation through Sephadex G-50 Superfine resin, and sequences were analyzed with an ABI Prism 3700 apparatus (Applied Biosystems). The sequences were aligned to the genomic sequence of RLTPR (Ensembl) with the CLUSTAL W2 multiple sequence alignment software.

RLTPR qRT-PCR

Total RNA was extracted from cell lines using the RNeasy Extraction kit (QIAGEN). RNA was reverse transcribed di-

rectly with the High Capacity RNA-to-cDNA Master Mix (Applied Biosystems). qRT-PCR was performed with an Assays-on-Demand probe/primer (Applied Biosystems) specific for RLTPR-FAM (HS00418748_m1) and β-glucuronidase-VIC (4326320E), which was used for normalization. Results are expressed according to the ΔΔCt (cycle threshold) method, as described by the manufacturer.

Plasmids, directed mutagenesis, transient transfection, and CARMIL three-dimensional (3D) structure model

The C-terminal Myc/DDK-tagged pCMV6 empty vector and the human *RLTPR* expression vector were purchased from OriGene (RC217662). Constructs carrying mutant alleles were generated from this plasmid by direct mutagenesis with a site-directed mutagenesis kit (QuickChange II XL; Agilent Technologies), according the manufacturer's instructions. For coimmunoprecipitation experiments, full-length *RLTPR* WT cDNA was subcloned into the V5/His-tagged pcDNA3.1 plasmid using the directional TOPO expression kit (Thermo Fisher Scientific). HEK293T cells were transiently transfected with the various constructs, using the Lipofectamine LTX kit (Thermo Fisher Scientific), according to the manufacturer's instructions. The 3D structure of the CARMIL LRR region was previously described (Zwolak et al., 2013). The 3D structure picture and mutations were displayed using Protein Workshop 4.2.0 (Moreland et al., 2005).

Cell lysis, immunoprecipitation, and immunoblotting

Total proteins were solubilized in extraction buffer (25 mM Tris-HCl, pH 7.6, 150 mM $NaCl_2$, 1% NP-40, 1 mM EDTA, 1× proteinase inhibitor cocktail mix, 1 mM PMSF, and 1 mM Na_3VO_4). Immunoblot analysis was performed using SDS-PAGE. Immunoblotting was performed using Ab against an N-terminal RLTPR peptide (E-15; Santa Cruz Biotechnology, Inc.), the C-terminal RLTPR peptide 1,186–1,310 (EM-53; Roncagalli et al., 2016), vinculin (EPR8185; Abcam), and GAPDH (FL335; Santa Cruz Biotechnology, Inc.). For coimmunoprecipitation experiments, V5-tagged and Myc/DDK-tagged RLTPR were cotransfected by X-tremeGENE 9 DNA transfection reagent (Roche) in HEK293T cells. Protein extracts were immunoprecipitated using anti-Myc (A-14; Santa Cruz Biotechnology, Inc.) and agarose A/G beads (Santa Cruz Biotechnology, Inc.) after a background-clearing step with an isotype control and agarose A/G beads (Santa Cruz Biotechnology, Inc.). Immunoprecipitated proteins were subsequently resolved on SDS-PAGE. Blots were probed with anti-DDK (TA50011-1; OriGene) and anti–V5-HRP (R962-25; Invitrogen) Abs.

Abs and flow cytometry

Immunophenotyping was performed by flow cytometry with mAbs against CD1c (L161; BioLegend), CD3 (7D6, Invitrogen; UCHT1, BD), CD4 (RPA-T4 or SK3; BD), CD8 (RPA-T8; BD), CD11c (S-HCL-13; BD), CD14 (M5E2; BD), CD16 (VEP13, Miltenyi Biotec; 3G8, BD), CD19 (4G7; BD), CD20 (LT20, Miltenyi Biotec; H1, BD), CD25 (MA-251; BD), CD27 (O323; Sony), CD28 (CD28.2; eBioscience), CD40L (89–76; BD), CD45RA (Hl100, BD; T6D11, Miltenyi Biotec), CD56 (B159 and NCAM16.2; BD), CD107a (H4A3; BD), CD123 (6H6; BioLegend), CD141 (1A4; BD), CD161 (DX12; BD), CCR7 (G043H7; Sony), CRTh2 (BM16; BD), ERK1/2 pT202/pY204 (20A; BD), FOXP3 (259D/C7; BD), HLA-DR (L243; BioLegend), ICOS (C398.4A), IkBα (25/IkBa/MAD-3; BD), P65 pS529 (K10-895.12.50; BD), RLTPR (EM-53; in house), TCR–iNKT cell (6B11; BD), TCR-γδ (11F2; Miltenyi Biotec), TCR-Vα7.2 (REA179; Miltenyi Biotec), TNF (cA2; Miltenyi Biotec), IFN-γ (B27; BD); IL-2 (MQ1-17H12; Sony); and Aqua Dead Cell Stain kit (Thermo Fisher Scientific). When required, after extracellular staining, cells were fixed and permeabilized using a fixation/permeabilization kit (eBioscience) before intracellular staining. Samples were acquired on a FACS Aria II, Fortessa X20 (BD), or Gallios (Beckman Coulter) flow cytometer depending on experiments. Identification of the different subsets for RLTPR expression analysis in the various leukocytes subsets of patients and controls was performed as followed after excluding dead cells: naive B cells ($CD19^+CD27^-$), memory B cells ($CD19^+CD27^+$), $CD56^{bright}$ NK cells ($CD3^-CD56^{bright}$), $CD56^{dim}$ ($CD3^-CD56^{dim}$), naive $CD4^+$ T cells ($CD3^+CD4^+CD45RA^+CCR7^+$), central memory $CD4^+$ T cells ($CD3^+CD4^+CD45RA^-CCR7^+$), effector memory $CD4^+$ T cells ($CD3^+CD4^+CCR7^-$), naive $CD8^+$ T cells ($CD3^+CD8^+CD45RA^+CCR7^+$), central memory $CD8^+$ T cells ($CD3^+CD8^+CD45RA^-CCR7^+$), effector memory $CD8^+$ T cells ($CD3^+CD8^+CCR7^-$), T reg cells ($CD3^+CD4^+CD25^{bright}FOXP3^+$), MAIT cells ($CD3^+CD161^+$TCR-$V\alpha7.2^+$), γδ T cells ($CD3^+$TCR-$\gamma\delta^+$), $CD16^+$ monocytes ($CD14^{dim}CD16^+$), $CD16^-$ monocytes ($CD14^{bright}CD16^-$), mDC1 ($Lin^-HLA\text{-}DR^+CD11c^+CD1c^+CD141^-$), mDC2 ($Lin^-HLA\text{-}DR^+CD11c^+CD1c^-CD141^+$), and plasmacytoid DCs ($Lin^-HLA\text{-}DR^+CD11c^-CD123^+$).

T cell–redirected functional assay

Thawed PBMCs were rested overnight in complete medium and distributed at a final concentration of 5×10^6 cells/ml in 96-well U-bottom plates. P815 mouse mastocytoma target cells were added to PBMCs at a final concentration of 2.5×10^6 cells/ml. Anti–CD3-PE or PE-Cy5.5 (7D6; 1/100) and/or anti-CD28 (CD28.2; 5 µg/ml) were added alone or in combinations in the indicated wells. The cells were incubated for 6 h at 37°C and 5% CO_2 after the addition of monensin (1/1,500 final concentration; GolgiStop; BD), brefeldin A (1/1,000 final concentration; GolgiPlug; BD), and CD107a-FITC (1/100 final concentration; H4A3). After incubation, cells were washed and stained for CD3, CD4, CD8, CCR7, CD45RA, and dead cells, permeabilized (fixation/permeabilization buffer; eBioscience), and stained for intracellular TNF (cA2; Miltenyi Biotec), IL-2 (MQ1-17H12; Sony), and IFN-γ (B27; BD) before analysis by flow cytometry.

Phospho–NF-κB p65 in PHA blasts

PHA blasts derived from patients' PBMCs were IL-2 starved 16 h before the assay. 10^6 cells were distributed in a 96-well V-bottom plate and stained on ice during 10 min with anti-CD2 (RPA2.10; eBioscience), CD28 (CD28.2; eBioscience), or CD3 (OKT3; eBioscience) mAb as indicated (5 µg/ml each). Cells were washed twice with cold medium, and a polyclonal goat anti–mouse Ig (BD) was added to each well (5 µg/ml) to cross-link activating receptors. 40 ng/ml PMA was used in separate wells as a positive control. After 20-min incubation at 37°C, cells were washed once with cold 1× PBS and then stained for 10 min on ice using the Aqua Dead Cell Marker kit (Thermo Fisher Scientific). Cells were fixed for 10 min at 37°C using Fix Buffer I (BD) and stained for 30 min with mAb against CD3 (BW264/56; Miltenyi Biotec), CD4 (M-T321; Miltenyi Biotec), and CD8 (BW135/80; Miltenyi Biotec). After extracellular marker staining, cells were permeabilized for 20 min at room temperatures using Perm Buffer III (BD) and stained for 3 h at room temperature with an IgG2b isotypic control or anti–NF-κB p65-(pS259)-PE (BD). Cells were subsequently acquired on a FACS Gallios flow cytometer and analyzed with FlowJo software (v10; Tree Star).

IκBα degradation, phospho-P65, and ERK1/2 in primary B cells after BCR and CD40 stimulation

Frozen PBMCs were thawed the day before the assay and cultivated overnight in complete medium. PBMCs were first stained for dead cells and washed, and 5×10^5 PBMCs were distributed in a 96-well V-bottom plate. Cells were stimulated or not stimulated with complete medium containing 100 ng/ml Mega CD40L (Enzo Life Sciences), 20 µg/ml $F(ab')_2$ fragment goat anti–human IgM (Jackson ImmunoResearch Laboratories, Inc.), or 40 ng/ml PMA. Optimal stimulation time points for each readout were selected based on prior kinetic experiments performed on control PBMCs. After 5 (p-ERK1/2 measurement)- or 35 (p-P65 and IκBα measurement)-min stimulation, cells were fixed by adding Fix Buffer I (1:1 volume; BD) and incubated 10 min at 37°C. Cells were then permeabilized for 20 min at room temperatures using Perm Buffer III (BD) and stained for 3 h at room temperature with anti-CD20 (H1; BD) and IgG2b isotypic control, anti–NF-κB P65-(pS259) (BD), anti-ERK1/2 pT202/pY204 (BD), or anti-IκBα (BD). Cells were subsequently acquired on a FACS Gallios flow cytometer and analyzed with FlowJo software (v10).

Ex vivo naive and effector/memory CD4$^+$ T cell stimulation

$CD4^+$ T cells were isolated as described previously (Ma et al., 2012, 2015). In brief, $CD4^+$ T cells were labeled with anti-CD4, anti-CD45RA, anti-CCR7, anti-CD127, and anti-CD25, and naive (defined as $CD45RA^+CCR7^+CD25^{lo}$ $CD127^{hi}$ $CD4^+$) T cells or effector/memory cells (defined as $CD45RA^-CCR7^{\pm}CD4^+$) were isolated (>98% purity) using a FACSAria flow cytometer. Purified naive or effector/memory $CD4^+$ cells were labeled with CFSE and cultured with T cell activation and expansion beads (anti-CD2/CD3/CD28; Miltenyi Biotec) for 4 d, and then, culture supernatants were assessed for secretion of the indicated cytokine by cytometric bead array.

In vitro differentiation of naive CD4$^+$ T cells

Naive $CD4^+$ T cells (defined as $CD45RA^+CCR7^+CD25^{lo}$ $CD127^{hi}$ $CD4^+$) were isolated (>98% purity) with the use of a FACSAria flow cytometer from healthy controls or patients. Cells were labeled with CFSE and then cultured under polarizing conditions, as previously described (Ma et al., 2012). In brief, cells were cultured with T cell activation and expansion beads (anti-CD2/CD3/CD28; Miltenyi Biotec) alone or under Th1 (20 ng/ml IL-12; R&D Systems), Th2 (IL-4), or Th17 (TGFβ, IL-1β [20 ng/ml; PeproTech], IL-6 [50 ng/ml; PeproTech], IL-21 [50 ng/ml; PeproTech], IL-23 [20 ng/ml; eBioscience], anti–IL-4 [5 µg/ml], and anti–IFN-γ [5 µg/ml; eBioscience]) cell polarizing conditions. After different times, the cells and culture supernatants were harvested and assessed for proliferation by assessing dilution of CFSE or expression of CD40L or ICOS by flow cytometry, secretion of the indicated cytokines by cytometric bead array or ELISA, or expression of *TBX21*, *GATA3*, *RORC*, *BCL2*, *BCL2L1*, or *BCL2L11* by qRT-PCR as previously described (Ma et al., 2016).

Retrovirus production and transduction

Retroviral vectors pLZRS-IRES-ΔNGFR (empty vector) and pLZRS-IRES-RLTPR-ΔNGFR, both including a puromycin resistance cassette, were generated as previously described (de Paus et al., 2013). The ΔNGFR open reading frame encodes a truncated nerve growth factor receptor (NGFR; also known as CD271) protein that cannot transduce signals and in this system serves as a cell surface tag. In brief, 10 µg of vector pLZRS-IRES-ΔNGFR or pLZRS-IRES-WT-ΔNGFR were transfected into Phoenix A packaging cells using X-tremeGENE 9 DNA reagent (Roche) following manufacturer specifications. Positively transfected cells were selected with puromycin (Gibco) at a concentration of 2 µg/ml until all of them were positive for the surface expression of ΔNGFR as assessed by FACS with PE–anti-NGFR staining (BD). Phoenix A cells were then split in two flasks, and media was replaced. After 24 h, supernatant was collected, and retroviral particles were concentrated using Retro-X concentrator (Takara Bio Inc.) following the manufacturer's instructions. 10^7 herpesvirus saimiri T cells were mixed with retrovirus containing supernatant in a total volume of 6 ml. After 5 d, stably transduced cells were purified by magnetic-activated cell sorting using magnetic bead–conjugated anti-NGFR Ab (Miltenyi Biotec) following the manufacturer's protocol.

Auto-Ab testing

Serum samples from patients with *RLTPR* mutations were diluted 1:100 in PBS, and 100 µl of the dilution was incubated in duplicate with an autoantigen proteomic array (University of Texas Southwestern Medical Center Genomic and

Microarray Core Facility), which includes 94 self-antigens to analyze the frequency, antigen specificity, and isotype composition of auto-Abs. The list of the 94 antigens tested can be found on supplier's webpage. Plasma from two healthy control subjects and one patient with systemic lupus erythematosus served as negative and positive controls, respectively. The arrays were then incubated with Cy3-labeled anti–human IgG and Cy5-labeled anti–human IgA Abs, respectively, to define the IgG or IgA isotype specificity of the auto-Abs. Tiff images were generated by using a GenePix scanner (4000B; Molecular Devices) with laser wavelengths of 532 nm (for Cy3) and 635 nm (for Cy5) and analyzed with GenePix Pro software (6.0). Net fluorescence intensity (defined as the spot minus background fluorescence intensity) data obtained from duplicate spots were averaged. Data were normalized as follows. Across all samples, the Ig-positive controls (IgG or IgA) were averaged, and the positive controls in each sample were divided by the averaged positive control, generating a normalization factor for each sample. Each signal was than multiplied by the normalization factor for each block (sample). For each antigen, values from healthy donor samples were averaged. For each sample, ratios were then calculated between the value in the sample and the mean of values in healthy donors plus two SDs, thus defining relative auto-Ab reactivity (RAR) of the sample. RAR values >1 were considered positive. A heat map of the ratio values was generated by using MultiExperiment Viewer software (Dana–Farber Cancer Institute).

Whole-blood activation assays

Whole-blood assays were performed after 48-h stimulation as previously described (Feinberg et al., 2004): heparin-treated blood samples were stimulated in vitro with BCG (multiplicity of infection = 20; donated by C. Nathan, Weill Cornell Medical College, New York, NY) with or without 5,000 IU/ml IFN-γ (Imukin; Boehringer Ingelheim) or 20 ng/ml IL-12 (R&D Systems). Then, ELISA was performed on the collected supernatants, with Abs against IFN-γ or IL-12 (p40 and p70) and the human Pelipair IFN-γ kit (Sanquin) or the human Quantikine HS kit for IL-12 (R&D Systems). Levels of IL-6 and IL-10 secretion were determined with ELISA kits (M9316 and M1910; Sanquin) after 48-h incubation with the indicated agonists: 100 ng/ml of synthetic diacylated lipopeptide (PAM2CSK4, agonist of TLR2/6; InvivoGen), 10 ng/ml LPS (LPS Re 595 from *Salmonella minnesota*, agonist of TLR-4; Sigma-Aldrich), 20 ng/ml IL-1β (agonist of IL-1β receptor; R&D Systems), 10^7 part/ml of heat-killed *Staphylococcus aureus* (HKSA, recognized mainly by TLR2; InvivoGen), 100 ng/ml of synthetic triacylated lipoprotein (PAM3CSK4, agonist of TLR2/TLR1; InvivoGen), 1 µg/ml of purified lipoteichoic acid from *S. aureus* (agonist for TLR2; InvivoGen), and 10^{-7} M/10-5 M PMA/ionomycin (positive control; Sigma-Aldrich).

Statistics

For multiple group comparisons, one-way ANOVAs were applied. For single comparisons of independent groups, a Mann-Whitney test was performed. *, $P < 0.05$; **, $P < 0.01$; ***, $P < 0.001$. Analyses were performed using GraphPad Software.

Online supplemental material

Fig. S1 shows representative pictures of patients' skin phenotype. Fig. S2 shows genome-wide linkage analyses, conservation of L372 and L525 residues across species, and population genetics of *RLTPR*. Fig. S3 shows CD28 expression and co-stimulation in patients and controls. Fig. S4 shows auto-Abs against IL-17A, IL-17F, IFN-α, and IFN-γ in serum from RLTPR patients. Fig. S5 shows cytokine production in response to pathogen cytokines. Table S1 shows viral serologies and loads. Table S2 shows EBV PCR. Table S3 shows patients' immunophenotyping performed on whole-blood samples. Table S4 shows T cell proliferation. Table S5 shows immunoglobulins longitudinal follow up. Table S6, included in an Excel file, shows all rare (MAF <0.01) homozygous nonsynonymous coding variants.

ACKNOWLEDGMENTS

We would like to thank the patients and their families for their participation in this study. We thank John Hammer, James Gruschus, and Nico Tjandra for their input on the consequences of RLTPR mutations on the LRR structure. We thank the members of the laboratory, especially Ruben Barricarte-Martinez, for helpful discussions and Lahouari Amar, Yelena Nemirovskaya, Dominick Papandrea, Eric Anderson, Martine Courat, Céline Desvallées, and Michaëla Corrias for secretarial assistance.

This work was supported by grants from Institut National de la Santé et de la Recherche Médicale, Paris Descartes University, the French National Research Agency (ANR) under the Investments for the Future Program (grant ANR-10-IAHU-01), the National Agency for Research on AIDS and Viral Hepatitis (ANRS; grant ANRS-13292), the Rockefeller University, and the St. Giles Foundation. Y. Wang is supported by the ANRS (grant n°13318). E. Crestani is supported by the National Institute of Allergy and Infectious Diseases (educational grant 5T32AI007512). V. Béziat is supported by the ANR (grant ANR-13-PDOC-0025-01). S.G. Tangye and C.S. Ma were supported by the National Health and Medical Research Council of Australia. S.G. Tangye is also supported by the Australian-American Fulbright Commission. L.D. Notarangelo is supported by the National Institute of Allergy and Infectious Diseases (grant R01AI100887-01).

The authors declare no competing financial interests.

Submitted: 22 April 2016
Accepted: 17 August 2016

REFERENCES

Acuto, O., and F. Michel. 2003. CD28-mediated co-stimulation: a quantitative support for TCR signalling. *Nat. Rev. Immunol.* 3:939–951. http://dx.doi.org/10.1038/nri1248

Adzhubei, I.A., S. Schmidt, L. Peshkin, V.E. Ramensky, A. Gerasimova, P. Bork, A.S. Kondrashov, and S.R. Sunyaev. 2010. A method and server for predicting damaging missense mutations. *Nat. Methods.* 7:248–249. http://dx.doi.org/10.1038/nmeth0410-248

Alkhairy, O.K., R. Perez-Becker, G.J. Driessen, H. Abolhassani, J. van Montfrans, S. Borte, S. Choo, N. Wang, K. Tesselaar, M. Fang, et al. 2015. Novel mutations in TNFRSF7/CD27: Clinical, immunologic, and genetic characterization of human CD27 deficiency. *J. Allergy Clin. Immunol.* 136:703–712.e10. http://dx.doi.org/10.1016/j.jaci.2015.02.022

Alkhairy, O.K., H. Abolhassani, N. Rezaei, M. Fang, K.K. Andersen, Z. Chavoshzadeh, I. Mohammadzadeh, M.A. El-Rajab, M. Massaad, J. Chou,

et al. 2016. Spectrum of phenotypes associated with mutations in LRBA. *J. Clin. Immunol.* 36:33–45. http://dx.doi.org/10.1007/s10875-015-0224-7

Altin, J.A., L. Tian, A. Liston, E.M. Bertram, C.C. Goodnow, and M.C. Cook. 2011. Decreased T-cell receptor signaling through Card11 differentially compromises forkhead box protein 3–positive regulatory versus T_H2 effector cells to cause allergy. *J. Allergy Clin. Immunol.* 127:1277–1285.e5. http://dx.doi.org/10.1016/j.jaci.2010.12.1081

Aydin, S.E., S.S. Kilic, C. Aytekin, A. Kumar, O. Porras, L. Kainulainen, L. Kostyuchenko, F. Genel, N. Kütükcüler, N. Karaca, et al. Inborn errors working party of EBMT. 2015. DOCK8 deficiency: clinical and immunological phenotype and treatment options - a review of 136 patients. *J. Clin. Immunol.* 35:189–198. http://dx.doi.org/10.1007/s10875-014-0126-0

Azuma, M., J.H. Phillips, and L.L. Lanier. 1993. CD28$^-$ T lymphocytes: Antigenic and functional properties. *J. Immunol.* 150:1147–1159.

Belkadi, A., V. Pedergnana, A. Cobat, Y. Itan, Q.B. Vincent, A. Abhyankar, L. Shang, J. El Baghdadi, A. Bousfiha, A. Alcais, et al. Exome/Array Consortium. 2016. Whole-exome sequencing to analyze population structure, parental inbreeding, and familial linkage. *Proc. Natl. Acad. Sci. USA.* 113:6713–6718. http://dx.doi.org/10.1073/pnas.1606460113

Bennett, C.L., J. Christie, F. Ramsdell, M.E. Brunkow, P.J. Ferguson, L. Whitesell, T.E. Kelly, F.T. Saulsbury, P.F. Chance, and H.D. Ochs. 2001. The immune dysregulation, polyendocrinopathy, enteropathy, X-linked syndrome (IPEX) is caused by mutations of FOXP3. *Nat. Genet.* 27:20–21. http://dx.doi.org/10.1038/83713

Boise, L.H., A.J. Minn, P.J. Noel, C.H. June, M.A. Accavitti, T. Lindsten, and C.B. Thompson. 1995. CD28 costimulation can promote T cell survival by enhancing the expression of Bcl-XL. *Immunity.* 3:87–98. http://dx.doi.org/10.1016/1074-7613(95)90161-2

Buckley, R.H. 2004. Molecular defects in human severe combined immunodeficiency and approaches to immune reconstitution. *Annu. Rev. Immunol.* 22:625–655. http://dx.doi.org/10.1146/annurev.immunol.22.012703.104614

Bustamante, J., S. Boisson-Dupuis, L. Abel, and J.-L. Casanova. 2014. Mendelian susceptibility to mycobacterial disease: genetic, immunological, and clinical features of inborn errors of IFN-γ immunity. *Semin. Immunol.* 26:454–470. http://dx.doi.org/10.1016/j.smim.2014.09.008

Byun, M., C.S. Ma, A. Akçay, V. Pedergnana, U. Palendira, J. Myoung, D.T. Avery, Y. Liu, A. Abhyankar, L. Lorenzo, et al. 2013. Inherited human OX40 deficiency underlying classic Kaposi sarcoma of childhood. *J. Exp. Med.* 210:1743–1759. http://dx.doi.org/10.1084/jem.20130592

Casanova, J.L., and L. Abel. 2004. The human model: a genetic dissection of immunity to infection in natural conditions. *Nat. Rev. Immunol.* 4:55–66. http://dx.doi.org/10.1038/nri1264

Casanova, J.-L., M.E. Conley, S.J. Seligman, L. Abel, and L.D. Notarangelo. 2014. Guidelines for genetic studies in single patients: lessons from primary immunodeficiencies. *J. Exp. Med.* 211:2137–2149. http://dx.doi.org/10.1084/jem.20140520

Chang, T.T., C. Jabs, R.A. Sobel, V.K. Kuchroo, and A.H. Sharpe. 1999. Studies in B7-deficient mice reveal a critical role for B7 costimulation in both induction and effector phases of experimental autoimmune encephalomyelitis. *J. Exp. Med.* 190:733–740. http://dx.doi.org/10.1084/jem.190.5.733

Cosmi, L., F. Annunziato, M. Iwasaki, G. Galli, R. Manetti, E. Maggi, K. Nagata, and S. Romagnani. 2000. CRTH2 is the most reliable marker for the detection of circulating human type 2 Th and type 2 T cytotoxic cells in health and disease. *Eur. J. Immunol.* 30:2972–2979. http://dx.doi.org/10.1002/1521-4141(200010)30:10<2972::AID-IMMU2972>3.0.CO;2-#

de Paus, R.A., M.A. Geilenkirchen, S. van Riet, J.T. van Dissel, and E. van de Vosse. 2013. Differential expression and function of human IL-12Rβ2 polymorphic variants. *Mol. Immunol.* 56:380–389. http://dx.doi.org/10.1016/j.molimm.2013.07.002

Feinberg, J., C. Fieschi, R. Doffinger, M. Feinberg, T. Leclerc, S. Boisson-Dupuis, C. Picard, J. Bustamante, A. Chapgier, O. Filipe-Santos, et al. 2004. Bacillus Calmette Guérin triggers the IL-12/IFN-γ axis by an IRAK-4- and NEMO-dependent, non-cognate interaction between monocytes, NK, and T lymphocytes. *Eur. J. Immunol.* 34:3276–3284. http://dx.doi.org/10.1002/eji.200425221

Fleckenstein, B., and A. Ensser. 2004. Herpesvirus saimiri transformation of human T lymphocytes. *Curr. Protoc. Immunol.* Chapter 7:7.21.1–7.21.11. http://dx.doi.org/10.1002/0471142735.im0721s63

Foey, A.D., S.L. Parry, L.M. Williams, M. Feldmann, B.M. Foxwell, and F.M. Brennan. 1998. Regulation of monocyte IL-10 synthesis by endogenous IL-1 and TNF-α: role of the p38 and p42/44 mitogen-activated protein kinases. *J. Immunol.* 160:920–928.

Greil, J., T. Rausch, T. Giese, O.R. Bandapalli, V. Daniel, I. Bekeredjian-Ding, A.M. Stütz, C. Drees, S. Roth, J. Ruland, et al. 2013. Whole-exome sequencing links caspase recruitment domain 11 (CARD11) inactivation to severe combined immunodeficiency. *J. Allergy Clin. Immunol.* 131:1376–1383.e3. http://dx.doi.org/10.1016/j.jaci.2013.02.012

Hara, H., T. Wada, C. Bakal, I. Kozieradzki, S. Suzuki, N. Suzuki, M. Nghiem, E.K. Griffiths, C. Krawczyk, B. Bauer, et al. 2003. The MAGUK family protein CARD11 is essential for lymphocyte activation. *Immunity.* 18:763–775. http://dx.doi.org/10.1016/S1074-7613(03)00148-1

Hogan, L.H., W. Markofski, A. Bock, B. Barger, J.D. Morrissey, and M. Sandor. 2001. Mycobacterium bovis BCG-induced granuloma formation depends on gamma interferon and CD40 ligand but does not require CD28. *Infect. Immun.* 69:2596–2603. http://dx.doi.org/10.1128/IAI.69.4.2596-2603.2001

Huang, X., and W. Miller. 1991. A time-efficient, linear-space local similarity algorithm. *Adv. Appl. Math.* 12:337–357. http://dx.doi.org/10.1016/0196-8858(91)90017-D

Itan, Y., L. Shang, B. Boisson, E. Patin, A. Bolze, M. Moncada-Vélez, E. Scott, M.J. Ciancanelli, F.G. Lafaille, J.G. Markle, et al. 2015. The human gene damage index as a gene-level approach to prioritizing exome variants. *Proc. Natl. Acad. Sci. USA.* 112:13615–13620. http://dx.doi.org/10.1073/pnas.1518646112

Itan, Y., L. Shang, B. Boisson, M.J. Ciancanelli, J.G. Markle, R. Martinez-Barricarte, E. Scott, I. Shah, P.D. Stenson, J. Gleeson, et al. 2016. The mutation significance cutoff: gene-level thresholds for variant predictions. *Nat. Methods.* 13:109–110. http://dx.doi.org/10.1038/nmeth.3739

Jabara, H.H., T. Ohsumi, J. Chou, M.J. Massaad, H. Benson, A. Megarbane, E. Chouery, R. Mikhael, O. Gorka, A. Gewies, et al. 2013. A homozygous mucosa-associated lymphoid tissue 1 (MALT1) mutation in a family with combined immunodeficiency. *J. Allergy Clin. Immunol.* 132:151–158. http://dx.doi.org/10.1016/j.jaci.2013.04.047

Keles, S., L.M. Charbonnier, V. Kabaleeswaran, I. Reisli, F. Genel, N. Gulez, W. Al-Herz, N. Ramesh, A. Perez-Atayde, N.K. Eeder, et al. 2016. Dedicator of cytokinesis 8 regulates signal transducer and activator of transcription 3 activation and promotes T_H17 cell differentiation. *J. Allergy Clin. Immunol.* S0091-6749:30352–30359. http://dx.doi.org/10.1016/j.jaci.2016.04.023

Kircher, M., D.M. Witten, P. Jain, B.J. O'Roak, G.M. Cooper, and J. Shendure. 2014. A general framework for estimating the relative pathogenicity of human genetic variants. *Nat. Genet.* 46:310–315. http://dx.doi.org/10.1038/ng.2892

Kreins, A.Y., M.J. Ciancanelli, S. Okada, X.-F. Kong, N. Ramírez-Alejo, S.S. Kilic, J. El Baghdadi, S. Nonoyama, S.A. Mahdaviani, F. Ailal, et al. 2015. Human TYK2 deficiency: Mycobacterial and viral infections without hyper-IgE syndrome. *J. Exp. Med.* 212:1641–1662. http://dx.doi.org/10.1084/jem.20140280

Kuehn, H.S., W. Ouyang, B. Lo, E.K. Deenick, J.E. Niemela, D.T. Avery, J.-N. Schickel, D.Q. Tran, J. Stoddard, Y. Zhang, et al. 2014. Immune dysregulation in human subjects with heterozygous germline mutations in *CTLA4*. *Science.* 345:1623–1627. http://dx.doi.org/10.1126/science.1255904

Li, H., and R. Durbin. 2010. Fast and accurate long-read alignment with Burrows-Wheeler transform. *Bioinformatics.* 26:589–595. http://dx.doi.org/10.1093/bioinformatics/btp698

Li, H., B. Handsaker, A. Wysoker, T. Fennell, J. Ruan, N. Homer, G. Marth, G. Abecasis, and R. Durbin. 1000 Genome Project Data Processing Subgroup. 2009. The sequence alignment/map format and SAMtools. *Bioinformatics.* 25:2078–2079. http://dx.doi.org/10.1093/bioinformatics/btp352

Liang, Y., H. Niederstrasser, M. Edwards, C.E. Jackson, and J.A. Cooper. 2009. Distinct roles for CARMIL isoforms in cell migration. *Mol. Biol. Cell.* 20:5290–5305. http://dx.doi.org/10.1091/mbc.E08-10-1071

Liang, Y., M. Cucchetti, R. Roncagalli, T. Yokosuka, A. Malzac, E. Bertosio, J. Imbert, I.J. Nijman, M. Suchanek, T. Saito, et al. 2013. The lymphoid lineage-specific actin-uncapping protein Rltpr is essential for costimulation via CD28 and the development of regulatory T cells. *Nat. Immunol.* 14:858–866. http://dx.doi.org/10.1038/ni.2634

Ma, C.S., G.Y.J. Chew, N. Simpson, A. Priyadarshi, M. Wong, B. Grimbacher, D.A. Fulcher, S.G. Tangye, and M.C. Cook. 2008. Deficiency of Th17 cells in hyper IgE syndrome due to mutations in STAT3. *J. Exp. Med.* 205:1551–1557. http://dx.doi.org/10.1084/jem.20080218

Ma, C.S., D.T. Avery, A. Chan, M. Batten, J. Bustamante, S. Boisson-Dupuis, P.D. Arkwright, A.Y. Kreins, D. Averbuch, D. Engelhard, et al. 2012. Functional STAT3 deficiency compromises the generation of human T follicular helper cells. *Blood.* 119:3997–4008. http://dx.doi.org/10.1182/blood-2011-11-392985

Ma, C.S., N. Wong, G. Rao, D.T. Avery, J. Torpy, T. Hambridge, J. Bustamante, S. Okada, J.L. Stoddard, E.K. Deenick, et al. 2015. Monogenic mutations differentially affect the quantity and quality of T follicular helper cells in patients with human primary immunodeficiencies. *J. Allergy Clin. Immunol.* 136:993–1006.e1. http://dx.doi.org/10.1016/j.jaci.2015.05.036

Ma, C.S., N. Wong, G. Rao, A. Nguyen, D.T. Avery, K. Payne, J. Torpy, P. O'Young, E. Deenick, J. Bustamante, et al. 2016. Unique and shared signaling pathways cooperate to regulate the differentiation of human $CD4^+$ T cells into distinct effector subsets. *J. Exp. Med.* 213:1589–1608. http://dx.doi.org/10.1084/jem.20151467

Matsuzaka, Y., K. Okamoto, T. Mabuchi, M. Iizuka, A. Ozawa, A. Oka, G. Tamiya, J.K. Kulski, and H. Inoko. 2004. Identification, expression analysis and polymorphism of a novel *RLTPR* gene encoding a RGD motif, tropomodulin domain and proline/leucine-rich regions. *Gene.* 343:291–304. http://dx.doi.org/10.1016/j.gene.2004.09.004

McKenna, A., M. Hanna, E. Banks, A. Sivachenko, K. Cibulskis, A. Kernytsky, K. Garimella, D. Altshuler, S. Gabriel, M. Daly, and M.A. DePristo. 2010. The Genome Analysis Toolkit: a MapReduce framework for analyzing next-generation DNA sequencing data. *Genome Res.* 20:1297–1303. http://dx.doi.org/10.1101/gr.107524.110

McKinnon, M.L., J. Rozmus, S.-Y. Fung, A.F. Hirschfeld, K.L. Del Bel, L. Thomas, N. Marr, S.D. Martin, A.K. Marwaha, J.J. Priatel, et al. 2014. Combined immunodeficiency associated with homozygous MALT1 mutations. *J. Allergy Clin. Immunol.* 133:1458–1462.e7. http://dx.doi.org/10.1016/j.jaci.2013.10.045

McQuillan, R., A.-L. Leutenegger, R. Abdel-Rahman, C.S. Franklin, M. Pericic, L. Barac-Lauc, N. Smolej-Narancic, B. Janicijevic, O. Polasek, A. Tenesa, et al. 2008. Runs of homozygosity in European populations. *Am. J. Hum. Genet.* 83:359–372. http://dx.doi.org/10.1016/j.ajhg.2008.08.007

Medoff, B.D., B. Seed, R. Jackobek, J. Zora, Y. Yang, A.D. Luster, and R. Xavier. 2006. CARMA1 is critical for the development of allergic airway inflammation in a murine model of asthma. *J. Immunol.* 176:7272–7277. http://dx.doi.org/10.4049/jimmunol.176.12.7272

Milner, J.D., J.M. Ward, A. Keane-Myers, and W.E. Paul. 2007. Lymphopenic mice reconstituted with limited repertoire T cells develop severe, multiorgan, Th2-associated inflammatory disease. *Proc. Natl. Acad. Sci. USA.* 104:576–581. http://dx.doi.org/10.1073/pnas.0610289104

Milner, J.D., J.M. Brenchley, A. Laurence, A.F. Freeman, B.J. Hill, K.M. Elias, Y. Kanno, C. Spalding, H.Z. Elloumi, M.L. Paulson, et al. 2008. Impaired T_H17 cell differentiation in subjects with autosomal dominant hyper-IgE syndrome. *Nature.* 452:773–776. http://dx.doi.org/10.1038/nature06764

Mittrücker, H.-W., A. Köhler, T.W. Mak, and S.H.E. Kaufmann. 1999. Critical role of CD28 in protective immunity against *Salmonella typhimurium*. *J. Immunol.* 163:6769–6776.

Mittrücker, H.-W., M. Kursar, A. Köhler, R. Hurwitz, and S.H.E. Kaufmann. 2001. Role of CD28 for the generation and expansion of antigen-specific $CD8^+$ T lymphocytes during infection with *Listeria monocytogenes*. *J. Immunol.* 167:5620–5627. http://dx.doi.org/10.4049/jimmunol.167.10.5620

Montagnoli, C., A. Bacci, S. Bozza, R. Gaziano, P. Mosci, A.H. Sharpe, and L. Romani. 2002. B7/CD28-dependent $CD4^+CD25^+$ regulatory T cells are essential components of the memory-protective immunity to *Candida albicans*. *J. Immunol.* 169:6298–6308. http://dx.doi.org/10.4049/jimmunol.169.11.6298

Moreland, J.L., A. Gramada, O.V. Buzko, Q. Zhang, and P.E. Bourne. 2005. The Molecular Biology Toolkit (MBT): a modular platform for developing molecular visualization applications. *BMC Bioinformatics.* 6:21. http://dx.doi.org/10.1186/1471-2105-6-21

Nagata, K., K. Tanaka, K. Ogawa, K. Kemmotsu, T. Imai, O. Yoshie, H. Abe, K. Tada, M. Nakamura, K. Sugamura, and S. Takano. 1999. Selective expression of a novel surface molecule by human Th2 cells in vivo. *J. Immunol.* 162:1278–1286.

Ng, P.C., and S. Henikoff. 2001. Predicting deleterious amino acid substitutions. *Genome Res.* 11:863–874. http://dx.doi.org/10.1101/gr.176601

Notarangelo, L.D. 2014. Combined Immunodeficiencies with Nonfunctional T Lymphocytes. *In* Advances in Immunology. F.W. Alt, editor. Academic Press, Cambridge, MA. 121–190.

O'Shea, J.J., and W.E. Paul. 2010. Mechanisms underlying lineage commitment and plasticity of helper $CD4^+$ T cells. *Science.* 327:1098–1102. http://dx.doi.org/10.1126/science.1178334

Okada, S., J.G. Markle, E.K. Deenick, F. Mele, D. Averbuch, M. Lagos, M. Alzahrani, S. Al-Muhsen, R. Halwani, C.S. Ma, et al. 2015. Impairment of immunity to *Candida* and *Mycobacterium* in humans with bi-allelic RORC mutations. *Science.* 349:606–613. http://dx.doi.org/10.1126/science.aaa4282

Ozcan, E., L.D. Notarangelo, and R.S. Geha. 2008. Primary immune deficiencies with aberrant IgE production. *J. Allergy Clin. Immunol.* 122:1054–1062. http://dx.doi.org/10.1016/j.jaci.2008.10.023

Padigel, U.M., P.J. Perrin, and J.P. Farrell. 2001. The development of a Th1-type response and resistance to *Leishmania major* infection in the absence of CD40-CD40L costimulation. *J. Immunol.* 167:5874–5879. http://dx.doi.org/10.4049/jimmunol.167.10.5874

Pérez de Diego, R., S. Sánchez-Ramón, E. López-Collazo, R. Martínez-Barricarte, C. Cubillos-Zapata, A. Ferreira Cerdán, J.-L. Casanova, and A. Puel. 2015. Genetic errors of the human caspase recruitment domain-B-cell lymphoma 10-mucosa-associated lymphoid tissue lymphoma-translocation gene 1 (CBM) complex: Molecular, immunologic, and clinical heterogeneity. *J. Allergy Clin. Immunol.* 136:1139–1149. http://dx.doi.org/10.1016/j.jaci.2015.06.031

Picard, C., W. Al-Herz, A. Bousfiha, J.-L. Casanova, T. Chatila, M.E. Conley, C. Cunningham-Rundles, A. Etzioni, S.M. Holland, C. Klein, et al. 2015. Primary immunodeficiency diseases: an update on the classification from the international union of immunological societies expert committee for primary immunodeficiency 2015. *J. Clin. Immunol.* 35:696–726. http://dx.doi.org/10.1007/s10875-015-0201-1

Puel, A., C. Picard, M. Lorrot, C. Pons, M. Chrabieh, L. Lorenzo, M. Mamani-Matsuda, E. Jouanguy, D. Gendrel, and J.L. Casanova. 2008. Recurrent staphylococcal cellulitis and subcutaneous abscesses in a child with autoantibodies against IL-6. *J. Immunol.* 180:647–654. http://dx.doi.org/10.4049/jimmunol.180.1.647

Puel, A., S. Cypowyj, J. Bustamante, J.F. Wright, L. Liu, H.K. Lim, M. Migaud, L. Israel, M. Chrabieh, M. Audry, et al. 2011. Chronic mucocutaneous candidiasis in humans with inborn errors of interleukin-17 immunity. *Science.* 332:65–68. http://dx.doi.org/10.1126/science.1200439

Puel, A., S. Cypowyj, L. Maródi, L. Abel, C. Picard, and J.L. Casanova. 2012. Inborn errors of human IL-17 immunity underlie chronic mucocutaneous candidiasis. *Curr. Opin. Allergy Clin. Immunol.* 12:616–622. http://dx.doi.org/10.1097/ACI.0b013e328358cc0b

Punwani, D., H. Wang, A.Y. Chan, M.J. Cowan, J. Mallott, U. Sunderam, M. Mollenauer, R. Srinivasan, S.E. Brenner, A. Mulder, et al. 2015. Combined immunodeficiency due to MALT1 mutations, treated by hematopoietic cell transplantation. *J. Clin. Immunol.* 35:135–146. http://dx.doi.org/10.1007/s10875-014-0125-1

Purcell, S., B. Neale, K. Todd-Brown, L. Thomas, M.A.R. Ferreira, D. Bender, J. Maller, P. Sklar, P.I.W. de Bakker, M.J. Daly, and P.C. Sham. 2007. PLINK: a tool set for whole-genome association and population-based linkage analyses. *Am. J. Hum. Genet.* 81:559–575. http://dx.doi.org/10.1086/519795

Romero, P., A. Zippelius, I. Kurth, M.J. Pittet, C. Touvrey, E.M. Iancu, P. Corthesy, E. Devevre, D.E. Speiser, and N. Rufer. 2007. Four functionally distinct populations of human effector-memory $CD8^+$ T lymphocytes. *J. Immunol.* 178:4112–4119. http://dx.doi.org/10.4049/jimmunol.178.7.4112

Roncagalli, R., M. Cucchetti, N. Jarmuzynski, C. Gregoire, E. Bergot, S. Audebert, E. Baudelet, M. Goncalves Menoita, A. Joachim, S. Durand, et al. 2016. The scaffolding function of the RLTPR protein explains its essential role for CD28 costimulation in mouse and human T cells. *J. Exp. Med.*. http://dx.doi.org/10.1084/jem.20160579

Ruland, J., G.S. Duncan, A. Elia, I. del Barco Barrantes, L. Nguyen, S. Plyte, D.G. Millar, D. Bouchard, A. Wakeham, P.S. Ohashi, and T.W. Mak. 2001. Bcl10 is a positive regulator of antigen receptor-induced activation of NF-κ B and neural tube closure. *Cell.* 104:33–42. http://dx.doi.org/10.1016/S0092-8674(01)00189-1

Salzer, E., S. Daschkey, S. Choo, M. Gombert, E. Santos-Valente, S. Ginzel, M. Schwendinger, O.A. Haas, G. Fritsch, W.F. Pickl, et al. 2013. Combined immunodeficiency with life-threatening EBV-associated lymphoproliferative disorder in patients lacking functional CD27. *Haematologica.* 98:473–478. http://dx.doi.org/10.3324/haematol.2012.068791

Schubert, D., C. Bode, R. Kenefeck, T.Z. Hou, J.B. Wing, A. Kennedy, A. Bulashevska, B.-S. Petersen, A.A. Schäffer, B.A. Grüning, et al. 2014. Autosomal dominant immune dysregulation syndrome in humans with *CTLA4* mutations. *Nat. Med.* 20:1410–1416. http://dx.doi.org/10.1038/nm.3746

Scott, E.M., A. Halees, Y. Itan, E.G. Spencer, Y. He, M. Abdellateef, S.B. Gabriel, A. Belkadi, B. Boisson, L. Abel, et al. Middle East Variome Consortium. 2016. Capture of greater middle eastern genetic variation enhances disease gene discovery. *Nat. Genet.* In press.

Shahinian, A., K. Pfeffer, K.P. Lee, T.M. Kündig, K. Kishihara, A. Wakeham, K. Kawai, P.S. Ohashi, C.B. Thompson, and T.W. Mak. 1993. Differential T cell costimulatory requirements in CD28-deficient mice. *Science.* 261:609–612. http://dx.doi.org/10.1126/science.7688139

Shi, F.D., B. He, H. Li, D. Matusevicius, H. Link, and H.G. Ljunggren. 1998. Differential requirements for CD28 and CD40 ligand in the induction of experimental autoimmune myasthenia gravis. *Eur. J. Immunol.* 28:3587–3593. http://dx.doi.org/10.1002/(SICI)1521-4141(199811)28:11<3587::AID-IMMU3587>3.0.CO;2-Y

Stepensky, P., B. Keller, M. Buchta, A.-K. Kienzler, O. Elpeleg, R. Somech, S. Cohen, I. Shachar, L.A. Miosge, M. Schlesier, et al. 2013. Deficiency of caspase recruitment domain family, member 11 (CARD11), causes profound combined immunodeficiency in human subjects. *J. Allergy Clin. Immunol.* 131:477–485.e1. http://dx.doi.org/10.1016/j.jaci.2012.11.050

Stoletzki, N., and A. Eyre-Walker. 2011. Estimation of the neutrality index. *Mol. Biol. Evol.* 28:63–70. http://dx.doi.org/10.1093/molbev/msq249

Tada, Y., K. Nagasawa, A. Ho, F. Morito, O. Ushiyama, N. Suzuki, H. Ohta, and T.W. Mak. 1999. CD28-deficient mice are highly resistant to collagen-induced arthritis. *J. Immunol.* 162:203–208.

Tangye, S.G. 2014. XLP: clinical features and molecular etiology due to mutations in SH2D1A encoding SAP. *J. Clin. Immunol.* 34:772–779. http://dx.doi.org/10.1007/s10875-014-0083-7

Tangye, S.G., C.S. Ma, R. Brink, and E.K. Deenick. 2013. The good, the bad and the ugly - TFH cells in human health and disease. *Nat. Rev. Immunol.* 13:412–426. http://dx.doi.org/10.1038/nri3447

Tangye, S.G., B. Pillay, K.L. Randall, D.T. Avery, T.G. Phan, P. Gray, J.B. Ziegler, J.M. Smart, J. Peake, P.D. Arkwright, et al. 2016. DOCK8-deficient $CD4^+$ T cells are biased to a Th2 effector fate at the expense of Th1 and Th17 cells. *J. Allergy Clin. Immunol.* http://dx.doi.org/10.1016/j.jaci.2016.07.016

Thaker, Y.R., H. Schneider, and C.E. Rudd. 2015. TCR and CD28 activate the transcription factor NF-κB in T-cells via distinct adaptor signaling complexes. *Immunol. Lett.* 163:113–119. http://dx.doi.org/10.1016/j.imlet.2014.10.020

Torres, J.M., R. Martinez-Barricarte, S. García-Gómez, M.S. Mazariegos, Y. Itan, B. Boisson, R. Rholvarez, A. Jiménez-Reinoso, L. del Pino, R. Rodríguez-Pena, et al. 2014. Inherited BCL10 deficiency impairs hematopoietic and nonhematopoietic immunity. *J. Clin. Invest.* 124:5239–5248. http://dx.doi.org/10.1172/JCI77493

van Montfrans, J.M., A.I.M. Hoepelman, S. Otto, M. van Gijn, L. van de Corput, R.A. de Weger, L. Monaco-Shawver, P.P. Banerjee, E.A.M. Sanders, C.M. Jol-van der Zijde, et al. 2012. CD27 deficiency is associated with combined immunodeficiency and persistent symptomatic EBV viremia. *J. Allergy Clin. Immunol.* 129:787–793.e6. http://dx.doi.org/10.1016/j.jaci.2011.11.013

Wildin, R.S., F. Ramsdell, J. Peake, F. Faravelli, J.L. Casanova, N. Buist, E. Levy-Lahad, M. Mazzella, O. Goulet, L. Perroni, et al. 2001. X-linked neonatal diabetes mellitus, enteropathy and endocrinopathy syndrome is the human equivalent of mouse scurfy. *Nat. Genet.* 27:18–20. http://dx.doi.org/10.1038/83707

Zhang, Q., J.C. Davis, I.T. Lamborn, A.F. Freeman, H. Jing, A.J. Favreau, H.F. Matthews, J. Davis, M.L. Turner, G. Uzel, et al. 2009. Combined immunodeficiency associated with DOCK8 mutations. *N. Engl. J. Med.* 361:2046–2055. http://dx.doi.org/10.1056/NEJMoa0905506

Zhang, Q., H. Jing, and H.C. Su. 2016. Recent advances in DOCK8 immunodeficiency syndrome. *J. Clin. Immunol.* 36:441–449. http://dx.doi.org/10.1007/s10875-016-0296-z

Zhang, R., A. Huynh, G. Whitcher, J. Chang, J.S. Maltzman, and L.A. Turka. 2013. An obligate cell-intrinsic function for CD28 in Tregs. *J. Clin. Invest.* 123:580–593. http://dx.doi.org/10.1172/JCI65013

Zhang, Y., H.C. Su, and M.J. Lenardo. 2015. Genomics is rapidly advancing precision medicine for immunological disorders. *Nat. Immunol.* 16:1001–1004. http://dx.doi.org/10.1038/ni.3275

Zwolak, A., C. Yang, E.A. Feeser, E.M. Ostap, T. Svitkina, and R. Dominguez. 2013. CARMIL leading edge localization depends on a non-canonical PH domain and dimerization. *Nat. Commun.* 4:2523. http://dx.doi.org/10.1038/ncomms3523